Fluid Mechanics of Isolated Spiral Galaxies (revised 1/15/24)*

W. K. George† and T.G. Johansson‡
Gothenburg, Sweden

January 16, 2024

Abstract

By using integral techniques commonly applied to the averaged Euler equations used in fluid mechanics and turbulence, and treating the stars and dust separately, we show that there is no need for '**Dark Matter**' or '**Alternative Gravity**' to explain 'anomalous' galactic rotational velocities. They are not anomalous.

The integral momentum balance equation including source terms reduces to:

$$z_m(r)\left[V_\phi^2(r) - \frac{1}{2}r\frac{dV_r^2(r)}{dr}\right] = 4\pi G\int_0^r \langle\rho_{bar}(r')\rangle r'dr',$$

where r is the radial coordinate, $V_\phi(r)$ is the averaged azimuthal velocity, $V_r(r)$ is the averaged radial velocity, G is the gravitational constant, and $\langle\rho_{bar}(r)\rangle$ is the 'two-dimensional' baryonic density of stars and/or dust that is usually measured. We 'define' $z_m(r)$ to be '*the galaxy momentum thickness*'.

The mass source terms and coupling between stars and dust have been included in the V_r^2-contribution by using the mass conservation equation. Since the integral on the right-hand side is asymptotic to the total mass in the galaxy, say M_{tot}, clearly the left-hand-side must also approach a constant at large radius.

We also carry out an *equilibrium similarity analysis* which shows that there are two possible similarity regimes: one in which z_m is constant and V_ϕ is asymptotically constant; and the other in which z_m grows linearly with r and the velocities are power laws in r.

*This version differs from earlier posted versions in that two new appendices have been added: The previous Appendix B (similarity theory) is now Appendix C. The new Appendix B now discusses alternative derivations of our main equation using classical Bessel functions. And Appendix A 5 (Angular momentum) has been added. Other changes are mostly cosmetic or to fix typos. We expect to add in the near future a short section on M31 (Andromeda) and one showing that spherically symmetrical galaxies behave differently.

†email: georgewilliamk@gmail.com (Wiki: William K George) also Cambridge, MD USA
‡email: t.gunnar.j@gmail.com

We consider data from the Triangulum Galaxy (M33) and the Milky Way, both of which exhibit the star similarity solutions. Our rotational velocities computed from the integral equation above correspond well to both the shape and magnitude of the measurements, even at large radius. Both constant and power law regions are observed. The 'mean streamlines' computed from the velocity data for the Milky Way are virtually identical to log spirals, consistent with an equilibrium similarity analysis of the same equations.

"**At every crossroads on the path that leads to the future, tradition has placed 10,000 men to guard the past.**" Maurice Maeterlinck

Contents

List of Figures

Nomenclature

$\overline{q}$	q generic, overline used to indicate averaging over ϕ only
$\langle\,\rangle$	used to denote integration over z and averaging over ϕ
∇	gradient operator. In polar coordinates:$\partial/\partial r, (1/r)\partial\phi, \partial z$
δ	length scale as function of r
η	similarity coordinate;= $r/\delta(r)$
ρ	mass density,, usually as function of r, ϕ, z
ρ_s	similarity scale function for density defined by equation 37
ρ_{bar}	density of baryonic matter
$\hat{\rho}$	Fourier series coefficient of ρ_s, equation 170
$\overline{\rho}$	density integrated over z only, *equation* 167
$\overline{\overline{\rho}}$	density integrated over ϕ only, equation 206
$\langle\rho_{bar}\rangle$	integral of ρ_{bar} integrated over z and averaged over ϕ, defined by equation 203
ρ_{th}	top-hat baryonic density defined by equation 204
$\langle\rho_o\rangle$	density value at $r = 0$ in empirical fit of equations 56 - 59
σ_z	width in Gaussian curve fit, equation 206
σ	mass source in continuity equation 69
σ_L	integrated mass source contribution as function of r, equation 74
ϕ	azimuthal coordinate
ϕ_s	azimuthal position of streamline
Φ	Gravitation potential, solution to equation 1
Φ_s	gravitational similarity scale function of r, ϕ only, defined by equation 41
Φth	top-hat potential used for gradient only, equation 20
$\langle\Phi\rangle$	gravitational potential integrated over z and averaged over ϕ.
$\hat{\Phi}$	Fourier series coefficient of Φ_s, equation 169

A	similarity coeff. dependent on upstream conditions denoted by *, equation 183
B	similarity coeff. dependent on upstream conditions denoted by *, equation 184
b	coefficient
D	similarity coeff. dependent on upstream conditions denoted by *, equation 186
E	similarity coeff. dependent on upstream conditions denoted by *, equation 187
f_ρ	density similarity profile function of η only, defined by equation 37
$\vec{f}$	gravitational force vector defined by equation 2
F_r	radial velocity similarity profile function of η only, defined by equation 39
g	gravitation potential similarity profile function of η only, defined by equation 41
G	Universal gravitational constant
I_m	Modified Bessel function of Second Kind
K	similarity coeff. dependent on upstream conditions denoted by *, equation 42
K_m	Modified Bessel function of Second Kind
L_s	= Schwarzschild length scale for galazy, $2GM_{tot}/c^2$
m	Fourier component index in equations 169 and 170
$M_\odot$	Mass of the sun
M_g	Radial profile of baryonic mass of galaxy; equation 11
M_{tot}	Total baryonic mass of galaxy, equation 12
r	radial coordinate
r_s	streamline radial position
t	time, except when used as subscript with z_t where it is a density top-hat thickness
T_{ij}	instantaneous stress tensor,for continuum of interest
V_ϕ	azimuthal velocity
$V_{\phi th}$	azimuthal top-hat velocity defined by equation 17
$V_{s\phi}$	similarity scale velocity defined by equation 38
v_i	i^{th}-component of instantaneous velocity vector for continuum of interest
V_r	radial velocity
V_{rth}	radial top-hat velocity defined by equation 19
V_{sr}	similarity scale velocity defined by equation 39
V_z	velocity normal to plane of galaxy
V_{sz}	similarity scale velocity defined by equation 40
z	spatial coordinate perpendicular to plane of galaxy
z_m	momentum thickness defined by equation 26. Note also equation 32.
z_r	parameter in empirical fit to variation of $\langle \rho_{bar}(r) \rangle$ of equations 56-59
z_t	galaxy top-hat thickness defined by equation 204

1 Introduction

One of the great challenges for astronomers and physicists for the past 100 years has been the alleged existence of Dark Matter. The problem was first noticed by Zwicky[45], Oort [33] and with far more data Rubin et al. [35]. They noticed there did not seem to be enough matter in the galaxies they studied to support the gravitationally-dominated rotational motions they observed, and suggested the difference was due to *Dark Matter*. Dark Matter was presumed to be matter which did not admit light, but acted gravitationally like mass. Interest has expanded greatly since the Hubble telescope, and attention has expanded to include thousands of galaxies (e.g., McGaugh and coworkers [31]).

1.1 Some recent studies

Figure 1 shows a typical result for the galaxy labeled M33, the Triangulum Galaxy.[1] The difference between the velocity data labeled 'from starlight' and 'from 21 cm hydrogen' and that labeled 'Expected from visible disk' clearly present a problem. Since the velocities are much less than the speed of light, relativistic effects are negligible. So Newton's third law and Gauss gravitational law should apply. But apparently not – at least not without introducing matter we have not seen (Dark Matter). Or alternatively, changing the gravitational laws altogether (so-called Modified Gravity) so they behave differently at large distance.

While Dark Matter is surely a possible hypothesis, it is quite disconcerting that after nearly 100 years we have not found any. In fact the primary reason to infer it all seems to be the inability to balance the dynamical galaxy equations. We argue below that at least for galaxies, neither Dark Matter nor Modified Gravity are necessary. It is the solutions to equations from which the need has been inferred which are incorrect.

1.2 What are the 'galactic' equations that have been used

There are a number of approaches which have been applied, but all depend in one form or another on Gauss' gravitational law given by:

$$\nabla^2 \Phi_{bar} \;=\; 4\pi\, G\, \rho_{bar}, \tag{1}$$

where ∇^2 is the Laplacian operator, Φ_{bar} is the gravitational force potential, G is the universal gravitational constant, and ρ_{bar} is the density of the observable (or baryonic) matter. This Poisson equation constitutes the Gauss-Newton gravitational law. All researchers solve this equation (numerically or using empirical fits to the density) for all the matter they can infer from their telescopes. And they then calculate $\Phi_{bar}(\vec{x})$ for all space of interest.(Note that since the

[1] It was pointed out to us by one of the co-authors (E. Corbelli) of the data [7] that the axes of this very popular and much cited figure of unknown origin are improperly labeled. We use the correct data in Section 5 below.

galaxies are presumed to be in steady motion, only steady-state analysis is performed.) Then they calculate the gravitational force at any location by taking the negative of the gradient of Φ_{bar}; i.e.

$$\vec{f}(\vec{x}) = -\nabla\Phi_{bar}. \tag{2}$$

At this point approaches can differ slightly. Most (e.g., [31]) directly equate this force to compute the expected acceleration for motion in concentric circles, say V_ϕ^2/r, where V_ϕ is the azimuthal velocity and r is the distance from the center of rotation measured in cylindrical coordinates[2]. Thus they expect:

$$\frac{{V_\phi}^2}{r} \;=\; -\frac{d\Phi_{bar}}{dr}. \tag{3}$$

Figure 2 (used by permission) is from McGaugh et al. [31] shows plots of V_ϕ for three galaxies, along with the velocity inferred from the equations above using both two- and three-dimensional calculations *and a nominal assumed galaxy thickness*. It is the difference that is attributed to missing matter, or to alternative gravity. The lower part of the figure shows a remarkable correlation between the left-hand-side of equation 3 (referred to as g_{obs}) plotted versus the right-hand-side (referred to as g_{bar}) computed from equation 1 using an estimate of the density distribution.

An alternative approach incorporating both azimuthal and radial velocities was used by Eilers et al. [11] for the Milky Way. Equation 3 was replaced by Jeans Equation [26, 4] in the form:

$$\frac{\partial\nu\langle V_r^2\rangle}{\partial r} + \frac{\partial\nu\langle V_r V_z\rangle}{\partial z} + \nu\left(\frac{\langle V_r^2\rangle - \langle V_\phi^2\rangle}{r} + \frac{\partial\Phi}{\partial r}\right) = 0, \tag{4}$$

where $\nu(r)$ is the star density (corresponding to the $\langle\rho(r)\rangle$ which we will use later.) By neglecting the second term they solve this to obtain the square of a *'circular velocity'*, V_c^2, given by:

$$V_c^2(r) = \langle V_\phi^2\rangle - \langle V_r^2\rangle\left(1 + \frac{\ln\nu}{\ln r} + \frac{\ln\langle V_r^2\rangle}{\ln r}\right) = r\frac{\partial\Phi}{\partial r}\bigg|_{z=0}. \tag{5}$$

The radial profile of $V_c(r)$ computed from their measurements of the Milky Way is compared to the $r\,\partial\Phi/\partial r|_0$ computed from solving Laplace's equation, equation 1.

Our Figure 3 (Figure 1 of [11] reproduced here by permission) shows their velocity component measurements in the plane of the galaxy and their computed V_c. Our Figure 4 reproduces their Figure 3 which compares their circular velocities with those computed several ways from equation 5 using various assumed mass distributions including 'dark matter'. For the baryonic matter they simply assumed $\nu \propto \exp -r/r_o$ where $r_o = 3$ kpc.

[2]Note that in this paper we do NOT conform to the astrophysicists convention of using capital R for tbe distance from the center in cylindrical variables. Since we work only in cylindrical polar coordinates there should be no confusion.

Clearly none of the aforementioned efforts (or hundreds of others) succeed without invoking additional significant invisible or 'Dark Matter' to make up the short-fall. This is a common feature of almost all similar attempts for any galaxy – hence the label **'Galaxy Rotational Velocity Problem'**.

1.3 A fluid mechanics model for galaxies

In this paper we propose to use a fluid mechanics and continuum model, instead of the planetary and virial-based models reviewed briefly above. These are derived in detail in Appendix A. We use averaged continuum equations of momentum and mass conservation proposed originally by Euler (v. [2]). But unlike the usual application in gases or liquids, we use them in this context like a multi-phase flow where the 'fluid particles' are averages over many stars or clumps of dust. We assume that the stars and dust (or gas) can be treated separately. But since stars explode and new ones are formed we allow the equations for both dust and star equations to be coupled. We will focus entirely on the stars, and view the dust as both a source and a sink of mass and momentum.

As noted in Appendix A, we will ignore the higher order terms and 'Reynolds-type stresses' that arise when any averaging is applied to non-linear equations. Thus the equations and solutions we derive should be viewed in the same vein as the oft-used *geostrophic* approximations that have been so successful in describing the general features of ocean and atmospheric circulations. But might fail in a particular case because of the terms that have been neglected.

1.4 Galaxy 'streamlines'

A simple and early indicator of whether such an approach might succeed is to use the multi-component measurements of Eilers et al. [11] reproduced in Figure 3 above to produce mean streamlines of the fluid motion we believe is present.

A streamline in fluid mechanics is defined as a line everywhere tangent to the instantaneous velocity vector; i.e., if $d\vec{x}_s$ is a line element and $\vec{v}$ is the velocity vector, then the streamline is given by $d\vec{x}_s \times \vec{v} = 0$. The concept of a streamline using the mean flow (or *averaged* velocities) is more problematical, since the flow may never follow it. But sometimes it is useful for providing an overall picture, and this is one of those times. We can use the data of Figure 3 to compute the streamlines for the mean velocities as follows:

$$\frac{r_s \, d\phi_s}{V_\phi(r_s)} = \frac{dr_s}{V_r(r_s)}, \tag{6}$$

where the subscript 's' denotes the streamline coordinate. This can be integrated numerically using the data of [11] for V_r and V_ϕ. The result is plotted on Figure 5 superimposed on the picture of the Milky Way assembled from radiation data [39]. Note that we have computed both positive and negative legs to get both arms of the spiral. The overlay of the velocity results with the picture is quite spectacular. Hogg et al. [22] (in a related paper to [11]) show a

predominance of older stars at smaller radii, with newer stars being created at the outside. This would be consistent with an inward transport. In the same figure they include arrows showing the spatial distribution of velocities from which they computed the statistics.

Figure 6 shows two plots of streamlines: one (solid lines) using the same velocity data above but out to $r = 25$ kpc; the other (dashed lines) a true log-spiral given by:

$$r\, d\phi_s = 6.5\, dr, \tag{7}$$

or $\phi_s - \phi_o = 6.5 \ln r/r_o$. The picture overlay plot is limited by the picture to radial values of about $r = 10$ kpc, but this second plot goes out to 25 kpc.

Figure 7 shows a plot of V_ϕ/V_r using the same velocity data. It does appear that the data asymptotes to a constant, $V_\phi/V_r \approx 6.5$, hence the value of 6.5 used in Figure 6. This is a prediction of the similarity theory summarized in Section 3 (and derived in detail in Appendix C) which does not seem to have been noticed before.

Figure 8 shows radial profiles of the Eilers et al. [11] data for $V_\phi(r)$ and $V_r(r)$ (same as in Figure 3) but also plotting $V_\phi(r)/6.5$ on top of $V_r(r)$. This is not a fit to V_r, but even so is in reasonable agreement beyond $r = 5$ kpc. This is also a prediction of the similarity theory of Section 3 (and Appendix C) and does not seem to have been noticed before.

Interestingly, for the data plotted in the picture overlay plot of Figure 5, the velocity ratio is clearly still developing, but the velocity data still overlay the picture reasonably well. For values of $r > 10$, however, the log spiral curve in Figure 6 is almost indistinguishable from the streamlines computed from the velocity data. While none of these figures are 'proof' that the Milky Way is moving as a fluid continuum, the hypothesis surely merits serious consideration. We do that below and in the rest of this paper.

Part I: New Theory for Galaxies

In Part I we summarize the redevelopment of the basic equations. The details are largely in Appendices A and B. For the main body of the paper we restrict ourselves to statistically steady averaged motions, so all $\partial/\partial t$-terms of averages will be neglected. But in Appendix A we show how they could have been included.

2 Re-examining the 'Thin Disk' Equations

2.1 Mass distribution

The galaxy mass distribution as a function of radius r, say $M_g(r)$, is given by:

$$M_g(r) \;=\; \int_0^r dr'\, r' \int_0^{2\pi} d\phi \int_{-\infty}^{\infty} dz\, \rho_{bar}(r', \phi, z) \tag{8}$$

where $\rho_{bar}(r', \phi, z)$ is the density of baryonic matter (stars and dust) only expressed in cylindrical coordinates. The radial coordinate is r, the azimuthal coordinate, ϕ, and coordinate normal to the plane of the galaxy, z. Dark matter is not considered in the analysis below, nor is it needed to explain the galactic measurements considered.

For the remainder of this paper we define the symbols $\langle\ \rangle$ to mean integrating the quantity enclosed over z and averaging it over ϕ; i.e.,

$$\langle(\ )\rangle = \frac{1}{2\pi}\int_0^{2\pi} d\phi \int_{-\infty}^{\infty} dz\ (\ ), \tag{9}$$

where we invoke the convention that everything to the right of the integral sign and differential is to be integrated over that variable.

We define the two-dimensional density, $\langle\rho(r)\rangle$, to be the integral of $\rho_{bar}(r, \phi, z)$ across the galaxy in the z-direction and averaged azimuthally; i.e.,

$$\langle\rho(r)\rangle = \frac{1}{2\pi}\int_0^{2\pi} d\phi \int_{-\infty}^{\infty} dz\ \rho_{bar}(r, \phi, z), \tag{10}$$

So the mass contained inside radius r, say $M_g(r)$, is given by:

$$M_g(r) \quad = \quad 2\pi \int_0^r dr'\, r'\, \langle\rho(r')\rangle. \tag{11}$$

It follows that the total mass in the galaxy, say M_{tot}, is simply:

$$M_{tot} \quad = \quad 2\pi \int_0^{\infty} dr'\, r'\, \langle\rho(r')\rangle. \tag{12}$$

2.2 Mass conservation

In Appendix A2 we show that mass conservation in our 'thin disk' galaxy reduces to equations 73 rewritten here as:

$$r\langle\rho(r)V_r(r)\rangle = \sigma_L(r), \tag{13}$$

where we define, $\sigma_L(r)$ by:

$$\sigma_L(r) = \int_0^r \langle\sigma\rangle r' dr', \tag{14}$$

and $\langle\sigma\rangle$ is the net mass source integrated over z and averaged over ϕ. Note that $\sigma_L(r)$ and $\langle r\rho V_r\rangle$ have dimensions of mass per unit length per unit time, the latter because it has been integrated over z.

For the star mass and momentum balance equation, if the mass of stars being produced from dust is greater than the mass of dust being produced by them exploding, then both σ and σ_L are positive. Equation 13 and 14 are quite interesting and have profound implications for the relation between the radial

velocity, V_r, and the density. Since that discussion is tangential to our purpose here, we have included it as a part of Appendix A.2.

All of these source terms will be incorporated into the momentum equations below. Not surprisingly, they will be shown to only affect the radial velocity component, but in a very important way. We are not aware that the effect of these mass sources terms on the *momentum equation* has been previously noticed.

In parallel to the implications of mass conservation on the relation between density and radial velocity profiles, the assumed finiteness of total angular momentum in a galaxy places constraints on the interrelation of the profiles of azimuthal velocity and density. We defer this discussion to Appendix A.5, but note that whether the galaxy is flaring out or not is crucial in determining how fast the density falls and what asymptote the azimuthal velocity attains.

2.3 Momentum Conservation

There is a long history of treating 'thin shear layer" problems in Fluid Mechanics and especially turbulence (c. f. [17].) Basically the approach shows that entrainment is driven by weak pressure gradient resulting from the square of the cross-layer velocity, V_z^2, and the resulting streamwise pressure gradient is small (and usually can be neglected). The details of this are in Appendix A.3 where we show how to reduce Euler's equations for a fluid to the radial 'galaxy momentum equation', equation 83, given as:

$$\frac{\partial(\rho\, V_r)}{\partial t} + \frac{1}{r}\frac{\partial(r\rho V_r^2)}{\partial r} + \frac{1}{r}\frac{\partial(\rho V_\phi V_r)}{\partial \phi} + \frac{\partial(\rho V_r V_z)}{\partial z} - \rho\frac{V_\phi^2}{r}$$
$$= \frac{\partial}{\partial r}\left(\rho V_z^2\right) - \rho\,\frac{\partial \Phi}{\partial r} + \sigma V_r. \tag{15}$$

Note that the last term on the right-hand-side, σV_r, appears since we combined the momentum equation with the mass conservation times velocity in order to produce terms integrable over all the variables. It resembles closely the Jean's equation (e.g.used by [11, 3] but includes the $\partial V_z^2/\partial r$ which represents the second-order (and oft-neglected) pressure term. This is the classical thin-shear layer result commonly appearing in turbulent shear flows.

This particular form of Euler's equation can easily be integrated across the galactic disk, z and averaged azimuthally, ϕ. In Appendix A.4, by integrating over z and averaging over ϕ the equation above, we derived equation 84 as:

$$\frac{\partial\langle\rho\, V_r\rangle}{\partial t} + \frac{1}{r}\frac{\partial r\langle\rho V_r^2\rangle}{\partial r} - \frac{\partial}{\partial r}\langle\rho V_z^2\rangle - \frac{\langle\rho V_\phi^2\rangle}{r} = -\langle\rho\,\frac{\partial\Phi}{\partial r}\rangle + \langle\sigma V_r\rangle. \tag{16}$$

Note that every term is now enclosed in angle brackets (meaning it has been integrated over z and averaged over ϕ). Also note that the $\partial/\partial\phi$ and $\partial/\partial z$-terms have vanished identically, the former because of the assumed periodicity and the latter because the variables ρ and V_r are presumed zero above and below the galactic disk.

Now we make the following top-hat definitions:

$$\begin{aligned}
\langle \rho V_\phi^2 \rangle &= \langle \rho \rangle V_{\phi th}^2, && (17)\\
\langle \rho V_r^2 \rangle &= \langle \rho \rangle V_{rth}^2, && (18)\\
\langle \rho V_z^2 \rangle &= \langle \rho \rangle V_{zth}^2, && (19)\\
\langle \rho \, \frac{\partial \Phi}{\partial r} \rangle &= \langle \rho \rangle \frac{d\Phi_{th}}{dr}, && (20)
\end{aligned}$$

where 'th' means that we have replaced a z-profile by a single value that makes the definition correct.

Now let's consider what happens if we include the mass conservation equations at the end of Section 2.2. First let's examine the second term on the left-hand-side of equation 16; i.e., using our previous definition, $\langle r\rho V_r^2 \rangle = \langle r\rho \rangle V_{rth}^2 \approx \langle r\rho V_r \rangle V_{rth}$, then we can write:

$$\begin{aligned}
\frac{1}{r}\frac{\partial}{\partial r}\left(r\langle \rho V_r^2 \rangle\right) &\approx \frac{1}{r}\frac{\partial}{\partial r}\left(r\langle \rho V_r \rangle V_{rth}\right)\\
&\approx \frac{V_{rth}}{r}\frac{d}{dr}\left(r\langle \rho V_r \rangle\right) + \langle \rho V_r \rangle \frac{d}{dr} V_{rth}\\
&\approx V_{rth}\langle \sigma \rangle + \frac{\sigma_L}{r}\frac{d}{dr} V_{rth}, && (21)
\end{aligned}$$

where we have substituted using equations 13 and 14.

If we further assume that $\langle \sigma V_r \rangle \approx \langle \sigma \rangle V_r$, substitution yields:

$$\frac{\sigma_L}{r}\frac{d}{dr} V_{rth} - \frac{d}{dr}\langle \rho V_z^2 \rangle - \frac{\langle \rho V_\phi^2 \rangle}{r} = -\langle \rho \, \frac{\partial \Phi}{\partial r} \rangle. \qquad (22)$$

Note that we already assumed statistical stationarity for the continuity relation so we drop the time derivative here as well.

Substituting these into equation 22 and dividing by $\langle \rho \rangle$ and rearranging yields:

$$\begin{aligned}
\frac{d\Phi_{th}}{dr} &= \frac{V_{\phi th}^2}{r} - \frac{1}{\langle \rho \rangle}\left\{ \frac{\sigma_L}{r}\frac{dV_{rth}}{dr} + \frac{d}{dr}\left(\langle \rho \rangle V_{zth}^2\right)\right\}\\
&= \frac{V_{\phi th}^2}{r} - \frac{dV_{zth}^2}{dr} - V_{zth}^2 \frac{d}{dr}\ln\langle \rho \rangle - \left\{ \frac{\sigma_L}{r\langle \rho \rangle}\frac{dV_{rth}}{dr}\right\}. && (23)
\end{aligned}$$

Note that the V_r-derivatives have completely disappeared except for the source-dependent term. This is a direct consequence of using the integrated and azimuthally-averaged mass conservation equation.

Note that we will have a problem with the $\ln\langle \rho \rangle$ term if we use $\langle \rho \rangle \propto \exp(-r/R)$ since it will not go to zero like the other terms with increasing r.

But we have noted in Section 2.2 that this is not a good approximation except for purely circular motions, and it creates anomalies if used here (and probably by others as well). Nonetheless, as we shall see below, $V_z^2 << V_r^2 << V_\phi^2$, so the V_z^2-terms can be neglected even with an exponential density.

A power law density profile (or any combination of power-laws) creates no problems at all. We note (see Appendix A.5), however, that if the total angular momentum in the galaxy is finite, this places the additional constraint that $\langle \rho(r)\, V_\phi(r) \rangle$ must go to zero faster than $1/r^3$.

2.4 Gauss' Gravitational Law for Galaxies

Since the velocities are small compared to the speed of light, Gauss' gravitational law applies. In cylindrical polar coordinates it is given by:

$$\left[\frac{1}{r} \frac{\partial}{\partial r} r \frac{\partial}{\partial r} + \frac{1}{r^2} \frac{\partial^2}{\partial \phi^2} + \frac{\partial^2}{\partial z^2} \right] \Phi(r, \phi, z) = 4\pi\, G\, \rho(r, \phi, z), \tag{24}$$

where G is the universal gravitational constant. Like the momentum equation above, we deal with the averages of this equation in the main body of the text.

In Appendix A.6 we show this can be integrated over z and averaged over ϕ to obtain:

$$\frac{1}{r} \frac{d}{dr} \left(r \langle \frac{d}{dr} \Phi \rangle \right) = 4\pi\, G\, \langle \rho(r) \rangle, \tag{25}$$

since the other two terms integrate to zero. Note that all terms are now enclosed in angle brackets, $\langle\, \rangle$. This reduction of Gauss' gravitational law to a single dimension appears to be a major departure from previous analyses.

Now we define our 'momentum thickness', $z_m(r)$, by:

$$z_m(r)\ \frac{d\Phi_{th}(r)}{dr} = \frac{1}{2\pi} \int_0^{2\pi} d\phi \int_{-\infty}^{\infty} dz\ \frac{\partial \Phi(r, \phi, z)}{\partial r}. \tag{26}$$

So our gravitational law reduces to:

$$\frac{1}{r} \frac{d}{dr} \left[r \left(z_m \frac{d}{dr} \Phi_{th} \right) \right] = 4\pi\, G\, \langle \rho(r) \rangle. \tag{27}$$

Appendix B provides a detailed presentation of an alternative derivation of equation 25 using a clever approach to classical Fourier analysis and Bessel functions. The result is the same. The conditions for existence of the Fourier transforms are less general than the hypotheses made in this section, but the results are identical. Appendix B also shows a specific analytical solution (v. Fitzpatrick [37]) and uses it to show why previous calculations of galaxy gravitational potentials may have been in error.

2.5 Combining Gauss and Momentum Equations

Substituting from equation 23 yields:

$$\frac{1}{r}\frac{d}{dr}\left[r\left(z_m\left\{\frac{V_{\phi th}^2}{r}-\frac{dV_{zth}^2}{dr}-V_{zth}^2\frac{d}{dr}\ln\langle\rho\rangle-\left\{\frac{\sigma_L}{r\langle\rho\rangle}\frac{dV_{rth}}{dr}\right\}\right\}\right)\right]=4\pi\,G\,\langle\rho(r)\rangle. \tag{28}$$

(*Note that in addition to averaging the equations themselves across ϕ and integrating across z, this substitution appears to be the other crucial point of our departure from the traditional analysis. Our approach is a natural consequence of treating galaxies as fluid mechanics problems where the velocities and densities are themselves field properties.*)

Clearing the r terms in equation 28:

$$\frac{1}{r}\frac{d}{dr}\left(z_m\left[V_{\phi th}^2-r\frac{dV_{zth}^2}{dr}-rV_{zth}^2\frac{d}{dr}\ln\langle\rho\rangle-\frac{\sigma_L}{\langle\rho\rangle}\frac{dV_{rth}}{dr}\right]\right)=4\pi\,G\,\langle\rho(r)\rangle. \tag{29}$$

Note that $\sigma_L(r)$ is given by equation 14; so reversing the sides yields:

$$\sigma_L=r\langle\rho(r)V_r(r)\rangle\approx r\langle\rho(r)\rangle V_{rth}(r). \tag{30}$$

So if we know $\langle\rho\rangle$ and V_{rth}, we can determine σ_L.

Alternatively we can substitute equation 30 into equation 29 to obtain:

$$\frac{1}{r}\frac{d}{dr}\left(z_m\left[V_{\phi th}^2-\frac{1}{2}r\frac{dV_{rth}^2}{dr}-r\frac{dV_{zth}^2}{dr}-rV_{zth}^2\frac{d}{dr}\ln\langle\rho\rangle\right]\right)=4\pi\,G\,\langle\rho(r)\rangle. \tag{31}$$

This form is particularly nice since it includes the source terms implicitly in the dV_{rth}^2/dr-term. Note that if $dV_{rth}^2/dr<0$, $dV_{rth}^2/dr<0$ and $d\langle\rho\rangle/dr<0$ for large r, these extra terms act to decrease $z_mV_{\phi th}^2$ for any given density distribution on the right-hand-side.

Equation 31 can be integrated directly to obtain $z_mV_{\phi th}^2$ as:

$$z_m\left[V_{\phi th}^2-\frac{1}{2}r\frac{dV_{rth}^2}{dr}-r\frac{dV_{zth}^2}{dr}-rV_{zth}^2\frac{d}{dr}\ln\langle\rho\rangle\right]=4\pi\,G\int_0^r\langle\rho(r')\rangle r'dr'. \tag{32}$$

We shall argue below that the terms involving the transverse velocity, V_z are negligible. So to an excellent approximation, equation 32 reduces to:

$$z_m\left[V_{\phi th}^2-\frac{1}{2}r\frac{dV_{rth}^2}{dr}\right]\approx 4\pi\,G\int_0^r\langle\rho(r')\rangle r'dr'\;=\;2\,G\,M_g(r), \tag{33}$$

where we have used the definition of $M_g(r)$ in equation 11.

Moreover we shall see that away from the core (of spiral galaxies at least) $V_r^2<<V_\phi^2$ so this further reduces to:

$$z_m\;V_{\phi th}^2\approx 4\pi\,G\int_0^r\langle\rho(r')\rangle r'dr'=2\,G\,M_r(r). \tag{34}$$

A few things are obvious. Since the density on the right-hand-side can never be negative the left-hand can only increase or be asymptotically constant.

For very large values of r the integral is nearly constant so our expression reduces to:

$$z_m \; V_{\phi th}^2 \rightarrow 4\pi \, G \int_0^\infty \langle \rho(r') \rangle r' dr' = 2 \, G \, M_{tot}. \tag{35}$$

Before leaving this section we note what happens if we divide both sides of equation 35 by the square of the speed of light, say c^2:

$$\frac{V_\phi^2}{c^2} = \frac{\left(2GM_{tot}/c^2\right)}{z_m} = \frac{L_s}{z_m}. \tag{36}$$

The characteristic length scale, $L_s = 2GM_{tot}/c^2$, is usually referred to as the Schwarzschild 'radius', but here clearly has nothing to do with a 'radius'. Its appearance in this context is a bit surprising to say the least, especially in combination with the ratio V_ϕ^2/c^2 which is clearly relativistic and in a problem where we started in the non-relativistic limit.

Finally note that we could have followed others and defined an equivalent 'circular velocity', say V_c^2 using the bracketed terms on the left-hand-side of any of equations 32 - 35 above. In the application to the data below, the extra terms are negligible at least away from the center. The $\ln\langle\rho\rangle$ term is particularly problematical if used with exponential densities, since it causes the result to blow up with increasing r.

2.6 How to handle multiple phases?

One way to use the results derived in the preceding sections is to simply sum the densities of all the type of mass present (e.g. gas, stars, etc.), and compute a z_m for the mixture. Another alternative is to treat each phase separately by assuming for example that the gas and stars overlap each other, but interact only very weakly or at least rarely. In the absence of evidence to the contrary, both gas and stars could be assumed to move with the same averaged velocity. We shall show such results for M33. Obviously this will give a smaller value of $z_m(r)$ for each material considered than adding their densities together to get a single value.

Clearly the more detailed the information available, the more powerful the equations derived herein become. For example if the gas velocity profile is different than that of the stars, this will very much make their top-hat representatives different. For the most part in astronomical measurements, unlike most problems in Fluid Mechanics, there are no profiles, only integrated values. So we consider only the simplest cases below, and leave it for others to explore this treasure-trove of opportunities.

3 An Equilibrium Similarity Theory for Galaxies

The kind of results demonstrated above in Section 1.3 for the Milky Way have special significance to turbulence researchers; specifically:

- The streamline coincidence with what we see in the pictures (Figure 5).
- The success of a simple log spiral to account for the measured velocities away from the center (Figure 6).
- The possible asymptotic constancy of the velocity ratio (see Figure 7).

All of these suggest that we are looking at a turbulent shear flow and should seek an similarity solution of some type.

The most successful in terms of accounting for a wide-variety of flows and initial or upstream conditions has been **equilibrium similarity**. Equilibrium similarity is different from classical similarity in that the solutions can depend uniquely on initial conditions, unlike the so-called 'universal solutions' which dominated turbulence theories until the 1980's (and still dominate many texts). Basically 'equilibrium similarity' hypothesizes a single length scale, say δ, for which δ evolves in time or space. These solutions emerge after an initial adjustment region, and thereafter all the relevant terms in the equations stay in balance with each other (or until something makes them change). This generally requires that there is more than one velocity scale which differ by factors of the growth rate of the length scale.

Originally proposed by one of us (WKG [13], See also [15, 17]) the ideas have been applied to a wide variety of simple shear flows, homogeneous flows, and even by us to the universe [20]. Examples of applications to experiments include the two-dimensional wake of Johansson et al. [27] which showed how one solution can evolve downstream into another as new terms grow into the equation while others die out; or Shiri et al. [36] who explained how the rotation dies out faster than velocity in rotating jets. Wosnik and Dufresne [44] applied both ideas to turbulent swirling wakes, and Danaila et al. [10] extended it to variable viscosity jets. Moser et al. [32] had similar success explaining numerically generated wakes. One of the best examples is due to Rogers [34] who found 12 different solutions for a forced wake, each corresponding to how he forced the wake and which terms he turned on. Applications to wall-bounded flows include George et al. [18], Castillo and George [5], Castillo et al. [6], Wosnik et al. [43] and Hultmark [23]. All of these solutions have the common feature that it is the growth rate of the length scale that reflects the initial conditions and determines all the dependent variables. The velocity moments typically take longer than the length scale to reach their asymptotic state. Often (but not always) for turbulent free shear flows, this length scale grows linearly.

Implementation of an equilibrium similarity analysis is extremely tedious and requires seemingly endless applications of the chain-rule. Therefore we have chosen to include the complete development as Appendix C, and only summarize

the beginning and conclusions here. Basically, we seek an equilibrium similarity solution of the Euler-based averaged equations of Appendix A of the form:

$$\begin{aligned}
\rho(r,z,\phi) &= \rho_s(r,\phi)\, f_\rho(\eta), && (37)\\
V_\phi(r,z,\phi) &= V_{s\phi}(r,\phi)\, F_\phi(\eta), && (38)\\
V_r(r,z,\phi) &= V_{sr}(r,\phi)\, F_r(\eta), && (39)\\
V_z(r,z,\phi) &= V_{sz}(r,\phi)\, F_z(\eta), && (40)\\
\Phi(r,z,\phi) &= \Phi_s(r,\phi)\, g(\eta), && (41)
\end{aligned}$$

where η is defined to be:

$$\eta = \frac{z}{\delta(r)}. \qquad (42)$$

We have put all of the r and ϕ-dependence into the scale functions denoted by subscript 's', and all of the z dependence has been scaled by an r-dependent length scale $\delta(r)$. It will turn out that our $z_m(r)$ defined in Section 2.4 above is proportional to $\delta(r)$. Clearly the functions of η represent the z-dependent profiles which fan out (or in) if δ varies with r.

Note that up to this point we have simply been transforming the governing equations into different variables. Now we substitute these transformed dependent variables into the basic equations and ask whether there are conditions under which the governing equations, including Gauss' gravitational law, reduce to ordinary differential equations of $\eta = z/\delta(z)$ only. The "*equilibrium similarity*' part comes in when we demand that all the r and ϕ-dependent coefficients have the same r and ϕ-dependence. Physically this means that all the internal adjustments of the equations have been completed, and thereafter all terms evolve together. So this is making a physical statement about how the flow reaches an asymptotic state – if it does. **Note that if there are no such solutions we won't find any.** But if we do, history suggests that unlike the classical solutions, these we will find in nature.

Now we need to define the coefficients of our similarity relations which in principle could be galaxy specific; i.e., different for each one depending on its history and initial conditions. Since these are unknown, we denote this possible dependence by *. From all the sections of Appendix C taken together, the following conditions are necessary for an equilibrium similarity solution:

$$\left[\frac{V_{s\phi}^2}{V_{sr}^2}\right] = A(*), \tag{43}$$

$$\left[\frac{\partial}{\partial \ln r} \ln\left\{r\rho_s V_{sr}^2\right\}\right] = B(*), \tag{44}$$

$$\left[\frac{1}{\rho_s V_{sr}^2}\,\frac{\partial}{\partial \phi}\left\{\rho_s\, V_{s\phi}\, V_{sr}\right\}\right] = C(*), \tag{45}$$

$$\left[\frac{V_{sz}}{V_{sr}}\right] = D(*)\,\left[\frac{d\delta}{dr}\right], \tag{46}$$

$$\left[\frac{\Phi_s}{V_{s\phi}^2}\right] = E(*), \tag{47}$$

$$\delta(r) = K(*)\; r, \tag{48}$$

where $*$ denotes a possible dependence on unknown source conditions which are specific to each particular galaxy. In other words, this is not a universal solution, but each galaxy could have different values depending on its origin and history. Also note that the r independent variable in these solutions does not in general correspond to the actual position of the center of the galaxy, so a virtual origin might be needed because of the development distance needed to reach the equilibrium similarity state.

We note that we have determined in Appendix C that indeed conditions for an equilibrium similarity solution exist. And like all previous such solutions it is described by a single length scale, $\delta(r)$, and at least two velocity scales which differ by a factor of $d\delta/dr$ from each other (e.g., equations 43 and 46).

4 Combining both approaches

We consider separately the two similarity conditions identified above: $\delta \propto r$ ($K(*) \neq 0$) and $\delta = constant$ ($K(*) = 0$). The first will be seen to correspond approximately to the Milky Way, the second to the Triangumlum Galaxy.

First we note that the similarity constraints of the preceding section imply that all the terms in equation 16 are proportional to $V_{s\phi}^2/r$, so we do not need to consider them separately, only the leading term, V_ϕ^2; i.e.,

$$\frac{1}{r}\frac{d}{dr}\left[\delta(r)\; V_{\phi th}^2(r)\right] \approx 4\pi G\left[\delta(r)\,\rho_s(r)\right] = 4\pi G\,\langle \rho_{bar}(r)\rangle. \tag{49}$$

(In fact, away from the core region we shall see the contributions of the neglected terms are only about 3 %.)

We identify $z_m(r)$ of the integral equation analysis with the $\delta(r)$ of our similarity theory, and define:

$$\delta(r) = z_m(r). \tag{50}$$

Also the similarity results require that:

$$\Phi_s(r) \propto V_{s\phi}(r)^2 \;=\; \alpha(*)\,\rho_s(r)\,\delta(r)^2 \;=\; \alpha(*)\,\langle\rho(r)\rangle\,\delta(r), \tag{51}$$

where we have assumed $\Phi_s(r)$ $V_{s\phi}(r)$ and $\rho_s(r)$ to now have been averaged over ϕ. We define, $\alpha(*)$ to be the galaxy dependent coefficient of proportionality between the velocity squared and density times δ-squared. (Note that α has dimensions of velocity-squared divided by density times length-squared.) So we can use these functional forms hereafter interchangeably.

We can now rewrite equation 49 in two ways. Either as an equation for the three-dimensional density scale, ρ_s:

$$\frac{\alpha}{r}\frac{d}{dr}\left[\delta(r)^3\;\rho_s(r)\right] \approx 4\pi G\,[\delta(r)\,\rho_s(r)]. \tag{52}$$

Or as an equation for the two-dimensional density integrated across the layer, $\langle\rho(r)\rangle$:

$$\frac{\alpha}{r}\frac{d}{dr}\left[\delta(r)^2\;\langle\rho(r)\rangle\right] \approx 4\pi G\,\langle\rho(r)\rangle. \tag{53}$$

Alternatively, we can rewrite equation 49 as an equation for the velocity squared; i.e.,

$$\frac{1}{r}\frac{d}{dr}\left[\delta(r)\;V_{\phi th}^2\right] \approx 4\pi G\,\langle\rho(r)\rangle = 4\pi G\,\alpha\,\frac{V_{s\phi}(r)^2}{\delta(r)}. \tag{54}$$

All three of these can be solved analytically if δ is known.

Part II: Comparison with Astronomical Data

In Part II we consider recent data and compare it to the theory above for two galaxies: the Triangulum Galaxy (M33 shown in Figure 1 and the Milky Way (shown schematically in Figure 5).

5 Evaluation of theory using Corbelli et al. [9] data for the Triangulum Galaxy

We consider M33 first both because it seems the simplest and it provides the most detailed and tabulated results for the quantities we need, namely azimuthally averaged and integrated values for $\langle\rho\rangle$ and $V_{\phi th}$ (or something very close to it). These have been presented in numerous references by Corbelli and co-workers ([8, 9, 30]). We focus on the 2014 version since the data were so nicely tabulated. Unfortunately the radial velocity V_r is not provided. There appears to be evidence (v. [24]), however, that M33 is indeed a log-spiral. If so, our similarity theory above suggests that $V_r \propto V_\phi$, at least in any similarity regime. We shall see that there is a least one such region, and perhaps two.

Figure 9 shows how the running mass, $M_g(r)$, defined by equation 11 for stars and gas separately increases with radius. Both star and gas masses rise rapidly near the center but quickly flatten out. The total star mass in the galaxy obtained by integration using equation 12 is $4.6\times10^9\ M_\odot$. The total gas present similarly obtained is $1.6\times10^9\ M_\odot$.

Figure 10 shows the values of the momentum thickness, $z_m(r)$, computed using equation 34 for stars only using the measured values of $V_\phi(r)$ and the $M_g(r)$ distributions above. The straight (red) line indicates the low r similarity regime for which $z_m \propto r$; the other similarity regime corresponds to z_m asymptotically constant. The solid black line is an interpolation consistent with both fits, $z_m = 2.75(1 - exp(-r/1.8))$.

The gas momentum thickness (not shown) is very similar to the thicknesses suggested by [9], and is about a factor of three smaller than the star values. It has been observed that the gas is often in a thinner layer than the stars, so that is consistent. It has also been observed in many terrestrial turbulent flows that momentum thicknesses for shear layers tend to be considerably larger than density profiles. And it has been noted that top-hat estimates tend to produce larger values than more realistic profiles (e. g. Gaussian). Appendix C shows why this is true for a simple Gaussian profile. In the absence of detailed cross-galaxy profiles, we have no reason to believe these momentum thicknesses do not correspond to what we see – especially given the alternative is 'Dark matter' which we cannot see at all, or changing the laws of physics (e. g. alternative gravity).

Figure 11 shows how the V_ϕ data for $M33$ of Corbelli et al. [9] can be reconstructed from equation 34 using a constant value of $z_m = 2.75$ (dashed red line) and also the using composite fit $z_m = 2.75(1 - exp(-r/1.8))$ shown in Figure 10. The composite fit is excellent, but not unexpected given the fit to

$z_m(r)$ in the preceding figure using the same data. It would have been nice to have had data for V_r and some actual z-profiles so the top-hat profile values for velocities and z_m could have been confirmed directly from their definitions.

Figure 12 is a log-log plot of $V_\phi(r)$ showing two possible similarity regimes: one for small values of r with slope 0.4 corresponding to the region in which $z_m \propto r$; and the other of constant velocity corresponding to the region for which z_m is asymptotically constant. Both are consistent with the similarity theory of Section 3 and described in detail in Appendix C.

It is not entirely clear to us (at least) what is going on here to cause the transition from one equilibrium similarity state to another, but here are two possibilities. One possibility is that the mass integral is reaching its asymptote, so clearly the tails of the distribution become important. A second possibility is suggested by Figure 13 which shows a plot of the density ratio, $\langle\rho\rangle_{stars}/\langle\rho\rangle_{gas}$. If star formation is related to the relative concentrations as suggested by Misiriotis et al. [25], then clearly when they are nearly equal is where one might expect to find a transition — and we do. Our equations have used the coupling of V_r and sources to eliminate sources from appearing explicitly. So both similarity regimes could be active regions of different star production/dissipation mechanisms, and the transition region where it switches.

6 Evaluation of theory using data of Eilers et al. [11] for the Milky Way

The Milky Way is a particularly interesting case since we know a lot about it, in part because we live in it. But being within a galaxy is not necessarily the best place to study it. We have leaned heavily on the excellent and comprehensive review by Bland-Hawthorne and Gerhart [3] and the careful exposition by Eilers et al. [11] and Hogg et al. [22] of their data. We do not attempt to repeat their historical summaries here, but instead focus only on the data they provided and the parameters required. Note that we used only their component velocities, except as noted in Figure 14.

We have already seen from the mean streamline plots of Figures 5 and 6 using the data of [11] that the Milky Way mean flow is a log-spiral. This was deduced from the similarity theory presented in Section 3 above (and Appendix B), and in particular the requirement that the ratio of V_ϕ/V_r be constant in any similarity regime. Figure 7 showed how this ratio varied with r. And Figure 8 showed the V_ϕ data divided by 6.5 and laid on top the of V_r-data. This does not seem to have been previously noticed, nor has its implications for the log spiral behavior. This should give considerable confidence as to both the quality of the data and the theory. It remains to see if the dynamical equations are satisfied, particularly equation 34.

Here are our assumed parameters, mostly from the afore-mentioned references:

$$
\begin{aligned}
M_{tot} &= 5 \times 10^{10}\,\mathrm{M}_\odot, && (55)\\
\langle\rho(r)\rangle &= \langle\rho_o\rangle\, e^{-r/z_r}, && (56)\\
2\,G\,M_{tot} &= 4.26 \times 10^5\ \mathrm{kpc(km/s)}^2, && (57)\\
z_r &= 3\ \mathrm{kpc} = 9,3 \times 10^{19}\,\mathrm{m}, && (58)\\
\langle\rho_o\rangle &= \frac{M_{tot}}{2\pi z_r^2} = 8.8 \times 10^8\,\mathrm{M}_\odot/\mathrm{kpc}^2 = 1.8 \times 10^0\ \mathrm{kg/m}^2, && (59)\\
\langle\rho_o\rangle\, G &= 1.2 \times 10^{-10}\,\mathrm{m/s}^2, && (60)
\end{aligned}
$$

where $M_\odot$ is the mass of the sun. M_{tot} is the value for the stellar baryonic matter suggested by Bland-Hawthorne/Gerhart [3], and the value of z_r is that chosen by Eilers et al.[11]. We have chosen $\langle\rho_o\rangle$ to produce the value of M_{tot} when substituted into equation 12. We note the following (for the non-astronomers reading this paper):

$$
\begin{aligned}
1\,\mathrm{kpc} &= 3.09 \times 10^{19}\,\mathrm{m}, && (61)\\
1\,\mathrm{M}_\odot &= 2 \times 10^{30}\,\mathrm{kg}, && (62)\\
G &= 6.7 \times 10^{-11}\,\mathrm{m}^3/(\mathrm{kg\ s}^2). && (63)
\end{aligned}
$$

For this particular choice of density (used by [11]), the defining integral for $M_g(r)$, equation 11 can be integrated analytically to yield:

$$
\frac{M_g(r)}{M_{tot}} = 1\ -\ (1 + r/z_r)\,\exp(-r/z_r). \qquad (64)
$$

Figure 14 shows the galaxy momentum thickness, $z_m(r)$, versus r computed using the the V_ϕ data from Figure 2 of [11], the mass distribution of equation 64 and equation 34. The zero intercept is about 3.6 kpc; z_m then rises linearly thereafter to about 14 kpc at $r = 25$ kpc. These seem quite a bit higher than expected, but note the difference near $r = 0$ from the M33 data in the previous section. For M33, $z_m(r)$ drops quickly to $z_m(0) \approx 0$ as $r \to 0$. But z_m for the Milky Way seems to be asymptotic to a constant value of about 3.6, and this offset is maintained throughout as the galaxy fans out. So perhaps we should have confined our attention to $r > 5$ kpc as did [11, 22] by only evaluating the integrals above this value. We noted above for M33 that these are 'top-hat' values computed from a velocity profile that is probably closer to a Gaussian, and that this could account for a factor of about 2.5. (Appendix C shows that a top-hat thickness over-estimates a Gaussian width parameter by about $\sqrt{2\,\pi}$ or about 2.5.) Also these are 'momentum' thicknesses, which on terrestrial flows tend to be larger than their density counterparts.

Finally note that the limiting values for large radius of $z_m\,V_\phi^2$ are directly proportional to the total galactic mass, M_{tot} in equation 35. Although in the spirit of 'dark matter', a suggestion of 'negative matter' to reduce z_m while conserving momentum is of course ridiculous. **So if z_m is too large, it means**

that the estimate of the total star mass is TOO LARGE – the exact opposite of previous inferences that there was not enough mass to support the galaxy gravitationally. Typical error estimates for baryonic mass are ±30% , although [3] suggest ±20% for the estimate we used from them. So the z_m estimates could be substantially smaller (but also larger).

The best linear fit is $z_m = 3.6 + 0.4\,r$ where length is in kpc. Also shown on the plot are the values of z_m using the values tabulated by Eilers et al. of their 'circular' velocity. The difference is primarily due to the misbehavior of their $\ln\langle\rho\rangle$ term if substituted for with an exponential. By incorporating mass conservation and neglecting V_z^2 we avoid this problem. Even so, in spite of the fact different equations were used and their very different origins, the two different methodologies give remarkably close estimates of the momentum thickness $z_m(r)$. Both lead to the conclusion that this galaxy must fan out to conserve momentum.

The fanning out for increasing values is consistent with the observations [3] (Section 5). Note that by definition, these values of $z_m(r)$ reproduce exactly the azimuthal velocity profile using the assumed density profile. This is demonstrated in Figure 16 which uses the linear fit to z_m and the same $M_g(r)$ in equation 34 to produce the velocity, V_ϕ. The fanning out of the galaxy with the nearly linear increase in $z_m(r)$ with radius is of course the reason for the decreasing values for V_ϕ with radius. This is surely not an independent verification, but re-assuring nonetheless. Only by producing actual profiles of V_ϕ which can be integrated across the layer can we have absolute confirmation of the approach. **Clearly no dark matter is required to produce the observed velocities if the galaxy is fanning out with increasing radius as suggested from our analysis and the data.**

The similarity solution requires that V_ϕ and V_r be either constant or power laws. Figure 16 shows a log-log plot of V_ϕ and V_r. The former clearly could be a power law, while for V_r it is acceptable. Figure 17 shows the same data on a linear-linear plot along with various fits to different regions. Eilers et al. [11] fitted a straight line to their circular velocity between $5 < r < 20$ (kpc). We show a similar straight line here on V_ϕ along with the power-law fit ($V_\phi = 264\ r^{-0.08}$). Both are acceptable.

Figure 18 plots $V_\phi(r)$, $M_g(r)$ and $z_m(r)$ together, and shows how the various regions for the range of z_m and the power law region of V_ϕ correspond to each other. They clearly overlap, and in a region where the mass integral is continuing to increase. It is important to remember (as we noted for M33 above) that in our formulation, we have accounted for the relation of V_r and any mass source terms – and they canceled each other out. So this could be a region of substantial star production/dissipation.

There is one more piece of information we can glean from the review paper of [3]. Since we are in our galaxy they were able actually to directly measure the z-dependent density profile for the Milky Way at our location near $r = 7.8$ kpc. By fitting a Gaussian profile, $\overline{\rho}(z) \propto \exp(-z^2/2\sigma_z^2)$ to the plot we deduce that $\sigma_z \approx 0.33$. Using equation 208 from Appendix D, the corresponding top-hat thickness is:

$$z_m = \sqrt{2\pi}\ \sigma_z \approx 0.83\ kpc. \tag{65}$$

So the factor of approximately 2.5 between our momentum thickness value, z_m, and previous estimates of galaxy thickness using densities seems quite reasonable. It is also important to note that whatever the actual factor is, it is nearly independent of radius.

It might be argued that we have simply replaced *Dark Matter* by another unknown quantity, $z_m(r)$. The difference is that $z_m(r)$ is not dark; we can quite literally see that galaxies have a thickness. And it has also been noted that they fan out, although with the exception of [9] to our knowledge this does not seem to have been considered dynamically important. Moreover our equations can be checked directly if z-profiles ever become available.

Finally, given our method of analysis since we actually compute $z_m(r)$ from the measurements, the velocity profiles are fitted exactly; so the motivating dilemma for Dark Matter for the past century disappears entirely. Moreover, if we could measure actual (instead of integrated) velocity profiles, we could calculate everything from them. This is the main reason integrated length scales have a long (and at times tortured) history in fluid mechanics (see for example the review of [14]).

7 Summary and Conclusions

Over the past 100 years and especially recently, the idea of Dark Matter has been introduced to explain a variety of astronomical anomalies. In this paper we have shown that there is another alternative to Dark Matter to explain the rotational velocity of galaxies – at least some of them, and maybe all. We began in the same place as most previous studies, with Newtonian dynamics in cylindrical coordinates and the Gauss gravitational law. We imagined an isolated galaxy to be a continuum. and its 'fluid particles' to be comprised of thousands of stars plus gas. We departed from conventional approaches (for the last 100 years) by integrating the equations (in this case the Reynolds-averaged Euler equations) over the galaxy thickness. We consider this a "thin-disk" approximation, but there is no reason for it to be. We also considered only velocities and densities which had been integrated over the galaxy thickness, since that corresponded to most of the data. And we considered only statistically stationary flows in time, although that assumption could be relaxed as well.

Our primary results are given by equations 32 – 35. Equation 34 is repeated here:

$$z_m \left[V_{\phi th}^2 - \frac{1}{2} r \frac{dV_{rth}^2}{dr} \right] \approx 4\pi\, G \int_0^r \langle \rho(r') \rangle r' dr' \ = \ 2\, G\, M_g(r). \tag{66}$$

The neglected terms, at least away from the core, involve only the cross-disk velocity, V_z^2, which is presumed much smaller (by a factor of $d\delta/dr$ from the similarity theory) than the radial component, V_r^2, which is in turn much smaller

than V_ϕ^2, by the same factor. We also showed that any production or dissipation of star matter is accounted for in the $V_r(r)$-term and its coupling to the mass conservation equation. These inclusions of the mass-conservation terms and V_z^2 terms and their integration across the galactic disk are the main reason for the difference from the commonly used Jeans equation.

So to leading order these equations are simply a balance between the square of the azimuthal velocity times the momentum thickness, $z_m\, V_\phi^2$, and $2\,G\,M_g(r)$ where M_g is the running mass integral. The most important difference is the appearance of the momentum thickness, $z_m(r)$, on the left-hand side of all the equations. It is no small curiosity that for very large values of r, dividing both sides of equation 35 by the speed of light squared leads to the following relationship:

$$\frac{V_\phi^2}{c^2} \approx \frac{R_s}{z_m}, \tag{67}$$

where $R_s = 2GM_{tot}/c^2$ is the Schwarschild radius defined using the total mass of the galaxy. There is probably no more significance to this than that it is dictated by dimensional consideration alone. But it is intriguing nonetheless, especially since the entire analysis is non-relativistic.

These equations seem to provide an excellent descriptions of both the Triangulum (M33) galaxy and the Milky Way **without needing to invoke Dark Matter**. And both galaxies are consistent with inferences from the equilibrium similarity solution described in detail in Appendix B. If sufficient profile information were available to perform the integrals defining the top-hat parameters directly, the theory could be better quantified. In fact, only after this is done could the theory be considered verified, a clear challenge to the astronomers.

Even though we began with Newton's and Gauss' laws (in continuum form), our resulting equations are quite different from the Kepler planetary-type laws that have been previously applied. Exactly why our approach gives different answers is not easily obvious, but we did try to make a 'guess' in Appendix B.6. Instead of solving a two- or three-dimensional Poisson' equation using an inferred or measured three-dimensional density, we avoided this problem entirely by integrating Gauss' equation across the layer and averaging azimuthally first. Then we substituted the momentum equation into it. The complications and difficulties of integrating Poisson's equation (or ANY equation involving a Laplacian) in an infinite environment were well-known to the generation of fluid mechanicians and physicists trained before computers were employed – meaning us[3]. We knew well the theorems of Potential Theory about sensitivity to boundary conditions, and that in fact the determination of the solution instantaneously everywhere by them. Perhaps these lessons have been forgotten. Or maybe we were just lucky to have followed a different path – the one advantage of coming from a different background. (Interestingly the final result of equation 34 was our first guess back in 2018.)

[3]We are both near 80 and were educated before computers dominated science education.

Integral equations have a long history – at least in fluid mechanics and turbulence. Both of us have been involved for five decades in unraveling and challenging measurements (and computations) of turbulent flows which were alleged to NOT satisfy the basic equations. Whether boundary layers or free shear flows, whether rotating or buoyancy-dominated, whether in the lab or in the atmosphere, in every case the problem was NOT because the data were wrong or that new physics were required (in spite of claims to the contrary). It was ALWAYS because the equations being used were wrong or being used incorrectly, or the experiment was not what it was believed to be (e.g.,[16]). From our perspective, that seems to be the case here: the astronomical experiments are marvelous – to we non-astronomers, incredible really. But the Kepler-like equations being used to explain them appear to have been both too simplistic and used incorrectly. And for sure the solutions of the Gauss gravitational laws could not have been correct.

We conclude this paper by remarking that while we have challenged the need for dark matter (at least for these two galaxies), there is much that needs to be done. This should enthuse the galaxy astronomical community. Freed from the tyranny of dark matter, there is much that should be investigated to fill in some of the gaps and possibilities we have identified above. Even the origins of galaxies can be re-examined using unsteady generalizations of our approach. This seems to be of special interest now given the recent discoveries by the James Webb Space Telescope. We do note in this context our as yet unpublished work on the expansion of the universe which suggests the universe is much older than previously believed (15.4 billion years versus 13.8 billion years)[20].

Acknowledgements

Our interest in this subject began during the Covid-19 period and was very much a result of discovering the arXiv papers by Eilers et al. [11] and McGaugh et al. [31]. Since neither of us any longer has a University affiliation we have had limited access to most sources. Without the availability of references on arXiv our contribution would not have been possible. Sadly (for us and the scientific community) arXiv considers this paper too novel and controversial, and has chosen to not make our work available to the scientific community. This is the second time for us, since our universe paper [20] received the same treatment. It would have been nice to have had an open discussion of both our ideas.

The Youtube lectures by Dr Becky (Smethurst) also contributed immeasurably to our thinking and understanding. Finally we acknowledge the important contribution of April D. Howard (artist and wife of WKG), both for putting up with years of listening to our failures, but most importantly for pointing out the similarity of our solutions to her Zentangle spirals and how she computed them. After this, everything fell into place, including recognizing the Milky Way's log-spiral behavior and for its implications about the possibility of a similarity solution.

Appendices

These Appendices contain most of the details of the analysis presented in the main body of the paper. For the most part the analysis is straight-forward, but at times tedious. Since few (even in Fluid Mechanics) aside from our own students seem to have been able to carry it out in other problems, we have tried to be complete and show each step. Portions will be nearly identical to the main body text, but this was necessary to maintain coherence.

A The equations of Newton-Gauss fluid mechanics

We hypothesize that we can treat the typical galaxy using 'continuum' mechanics. For the gas phase, this is obvious. For the stars the continuum hypothesis can be justified as follows. A characteristic length scale for gradients of averaged quantities near the center of a typical galaxy (like the Milky Way) is about 1 kpc. The Milky Way galaxy has about 10^7 stars in this region, and the core region has a volume of approximately 3 kpc^3 (3 kpc radius, 0.1 kpc thick). So about 3×10^6 stars per characteristic length, surely enough to treat it as a continuum. The number of stars per unit volume drops with increasing radius, but the length scales for changes with distance increases as well.

A.1 Reynolds-averaged momentum equation

But since the stars are not moving uniformly, even these 'continuum' motions are random, so we need to 'Reynolds-average' them. Reynolds-averaging in this context means imagining a finite number, say N, of statistically identical galaxies and averaging them in the limit as $N \to \infty$. In practice, this ensemble average is replaced by exploiting homogeneities in the spatial coordinates. So the appropriate equations are the averaged Euler's equations for a variable density flow dominated by gravity:

$$\overline{\rho \frac{Dv_i}{Dt}} = \overline{\frac{\partial T_{ij}}{\partial x_j}} - \overline{\rho \frac{\partial \Phi}{\partial x_j}}, \tag{68}$$

where ρ is the mass density, v_i is the instantaneous velocity, T_{ij} is the stress tensor, and Φ is the gravitational potential. The overline in this section denotes ensemble averages of the fluctuating quantities. Generally, the stress are negligible compared to the averaged velocity fluctuations (the so-called Reynolds stresses), except for the pressure which must be considered separately. But even the mechanical pressure it overwhelmed by the normal stresses from the fluctuating velocities. If we restrict to galaxies in near statistical equilibrium, we can eliminate the $\partial/\partial t$ of averaged quantities, but almost never the advective contribution, $v_j \partial/\partial x_j$,

A.2 Mass conservation

There is also an equation for mass conservation (often called the continuity equation) which with the same assumptions reduces to:

$$\frac{\partial \rho}{\partial t} + \frac{1}{r}\frac{\partial}{\partial r}(r\rho V_r) \; + \; \frac{1}{r}\frac{\partial}{\partial \phi}(\rho V_\phi) \; + \; \frac{\partial}{\partial z}(\rho V_z) \; = \; \sigma, \tag{69}$$

where σ represents sources or sinks per unit volume (like a blackhole in this context) or a distribution (from star creation for example if dust and stars are considered separately).

Integrating from $-\infty < z < \infty$ and averaging over ϕ yields:

$$\frac{1}{2\pi}\int_0^{2\pi} d\phi \int_{-\infty}^{\infty} dz \left\{ \frac{\partial}{\partial t}\rho + \frac{1}{r}\frac{\partial}{\partial r}(r\rho V_r) + \frac{1}{r}\frac{\partial}{\partial \phi}(\rho V_\phi) + \; \frac{\partial}{\partial z}(\rho V_z) \; - \; \sigma \right\} = 0. \tag{70}$$

Or equivalently, if (as in the main body of the paper) we use $\langle \; \rangle$ to represent the combined integration over z and averaging over ϕ:

$$\frac{\partial}{\partial t} r\langle\rho\rangle + \frac{\partial}{\partial r}\left[r\langle\rho V_r\rangle\right] + \frac{\partial}{\partial \phi}\langle\rho V_\phi\rangle + \left[\lim_{z\to\infty}(r\rho V_z) \; - \; \lim_{z\to-\infty}(r\rho V_z)\right] - r\langle\sigma\rangle = 0, \tag{71}$$

since the third and fourth terms inside the curly brackets are perfect differentials. The term ρV_z represents any entrainment and is zero only if it vanishes as $|z| \to \infty$; which we assume it does. If the galaxy is statistically stationary and azimuthally homogeneous or periodic by assumption, the first and third terms on the left-hand-side are also identically zero leaving:

$$\frac{d}{dr}\left[r\langle\rho(r)V_r(r)\rangle\right] \; - \; r\langle\sigma\rangle = 0. \tag{72}$$

We can integrate this directly to obtain:

$$r\langle\rho(r)V_r(r)\rangle = \sigma_L(r), \tag{73}$$

where we define, $\sigma_L(r)$ by:

$$\sigma_L(r) = \int_0^r \langle\sigma\rangle r' dr'. \tag{74}$$

Note that $\sigma_L(r)$ and $\langle r\rho V_r\rangle$ have dimensions of mass per unit time, the latter because it has been integrated over z.

Equation 73 is quite interesting and has profound implications. We consider three cases below.

- Case 1: No sources or sinks anywhere. $\sigma_L = 0$.

  This case is very interesting for what it implies about the flow. The only way to satisfy equation 73 for non-zero density and all r is for V_r to be

identically zero. This means flow in concentric circles – like planetary orbits. Alternatively, this condition could be satisfied by a ring vortex which could blow itself along.

- Case 2: A blackhole at the center: $\sigma_L = -\dot{M}_{bh}\,\delta(r)$ where $\dot{M}_{bh} = constant$ for a steady motion. Presumably $\dot{M}_{bh} > 0$ (meaning the blackhole is growing) and represents a sink, so $V_r < 0$ as well.

  If we substitute the two-dimensional delta function into equation 73 and integrate, for all $r > 0$ we obtain:

$$r\ \langle \rho(r) V_r(r) \rangle = -\dot{M}_{bh}. \tag{75}$$

  If $\dot{M}_{bh} > 0$ the continuous phase is losing mass. Note this is dimensionally correct since $\langle\ \rangle$ implies integration over z and averaging over ϕ, so there is an implicit z-thickness. If $\langle \rho(r) V_r(r) \rangle \approx \langle \rho(r) \rangle\ V_r(r)$, then for all $r > 0$:

$$r\ \langle \rho(r) \rangle V_r(r) = -\dot{M}_{bh} = constant. \tag{76}$$

  Now this result is interesting as well, since we know the right-hand side must be non-zero for the galaxy to spiral. But it is also especially interesting for what it implies about the frequent choice of $\langle \rho \rangle \propto exp(-r/R)$ where R is a galaxy disk width parameter. The velocity would have to blow up exponentially with increasing radius, i.e., $V_r \propto -1/r \times \exp(+r/R)$. So the positive exponent swamps the $1/r$ for large r. Clearly this can not be physical.

- Case 3: A distribution along r but no blackhole at center.

  In this case we must deal with the full integral for what ever distribution of σ_L is present. We shall see that this term seems to present the only possibility of making the velocity slowly decrease for constant thickness (like we see in the Milky Way).

- Case 4: Both a blackhole at the center and a distribution along r.

  This is probably what we need for the Milky Way since it both spirals and the asymptotic velocity drops off slowly.

A.3 Component Momentum conservation equations

The most convenient form of the momentum equation is obtained by combining Euler's equation with continuity. For the radial momentum this is done as follows:

$$\rho\left\{\frac{\partial V_r}{\partial t} + V_r\frac{\partial V_r}{\partial r} + \frac{V_\phi}{r}\frac{\partial V_r}{\partial \phi} + V_z\frac{\partial V_r}{\partial z} - \frac{V_\phi^2}{r}\right\}$$
$$+ V_r\left\{\frac{\partial \rho}{\partial t} + V_r\frac{\partial \rho}{\partial r} + \frac{V_\phi}{r}\frac{\partial \rho}{\partial \phi} + V_z\frac{\partial \rho}{\partial z}\right\}$$
$$+ \rho\left[\frac{1}{r}\frac{\partial}{\partial r}(r\,V_r) + \frac{1}{r}\frac{\partial V_\phi}{\partial \phi} + \frac{\partial V_z}{\partial z}\right] = -\frac{\partial P}{\partial r} - \rho\,\frac{\partial \Phi}{\partial r} - \sigma\,V_r, \quad (77)$$

where the second equation is obtained by simply multiplying the continuity equation by V_r. Note that we have included the mass source term. Adding these we get the momentum equation in a form we can integrate over z and ϕ as:

$$\frac{\partial(\rho\,V_r)}{\partial t} + \frac{1}{r}\frac{\partial(r\rho V_r^2)}{\partial r} + \frac{1}{r}\frac{\partial(\rho V_\phi V_r)}{\partial \phi} + \frac{\partial(\rho V_r V_z)}{\partial z} - \rho\frac{V_\phi^2}{r} \quad (78)$$
$$= -\frac{\partial P}{\partial r} - \rho\,\frac{\partial \Phi}{\partial r} + \sigma V_r.$$

We can similarly derive the azimuthal momentum equation as:

$$\frac{\partial(\rho\,V_\phi)}{\partial t} + \frac{1}{r}\frac{\partial(r\rho V_r V_\phi)}{\partial r} + \frac{1}{r}\frac{\partial(\rho V_\phi^2)}{\partial \phi} + \frac{\partial(\rho V_\phi V_z)}{\partial z} + \rho\frac{V_\phi V_r}{r} \quad (79)$$
$$= -\frac{1}{r}\frac{\partial P}{\partial \phi} - \frac{\rho}{r}\,\frac{\partial \Phi}{\partial \phi} + \sigma V_\phi.$$

And finally for the z-momentum equation:

$$\frac{\partial(\rho\,V_z)}{\partial t} + \frac{1}{r}\frac{\partial(r\rho V_r V_z)}{\partial r} + \frac{1}{r}\frac{\partial(\rho V_\phi V_z)}{\partial \phi} + \frac{\partial(\rho V_z^2)}{\partial z} \quad (80)$$
$$= -\frac{\partial P}{\partial z} - \rho\,\frac{\partial \Phi}{\partial z} + \sigma V_z.$$

A.4 Integrated momentum equations

We will ignore the time-derivative terms and assume our galaxy is statistically stationary. Now we want to substitute for the pressure in the radial-momentum equation using the results from the other two directions. First we rewrite the z-momentum equation, equation 80 to move the pressure to the left-hand side; i.e.,

$$\frac{\partial P}{\partial z} = -\rho\,\frac{\partial \Phi}{\partial z} - \frac{1}{r}\frac{\partial(r\rho V_r V_z)}{\partial r} - \frac{1}{r}\frac{\partial(\rho V_\phi V_z)}{\partial \phi} - \frac{\partial(\rho V_z^2)}{\partial z} + \sigma V_z. \quad (81)$$

Integrating over z:

$$P + \rho V_z^2 = \int_{-\infty}^{z} dz' \left\{ -\rho \frac{\partial \Phi}{\partial z'} - \frac{1}{r}\frac{\partial (r\rho V_r V_z)}{\partial r} - \frac{1}{r}\frac{\partial (\rho V_\phi V_z)}{\partial \phi} + \sigma V_z \right\} + function\ of\ r, \phi. \quad (82)$$

Note that ρV_z^2 also appears on the left-hand side.

In a typical turbulent thin-shear flow, the right-hand side of equation 82 is negligible. We assume that to be the case here; but note that we need to verify this *a posteriori*. Since there is presumed no flow and no pressure gradient outside the galaxy, the only streamwise pressure gradient inside the galaxy must be due only to the variation in the r-direction of ρV_z^2. So we can differentiate P with respect to r and substitute this into equation 79 to obtain to leading order:

$$\frac{\partial (\rho\, V_r)}{\partial t} + \frac{1}{r}\frac{\partial (r\rho V_r^2)}{\partial r} + \frac{1}{r}\frac{\partial (\rho V_\phi V_r)}{\partial \phi} + \frac{\partial (\rho V_r V_z)}{\partial z} - \rho \frac{V_\phi^2}{r} = \frac{\partial}{\partial r}\left[\rho V_z^2\right] - \rho \frac{\partial \Phi}{\partial r} + \sigma V_r. \quad (83)$$

We can integrate this over z and average over ϕ to obtain:

$$\frac{\partial \langle \rho\, V_r \rangle}{\partial t} + \frac{1}{r}\frac{\partial r \langle \rho V_r^2 \rangle}{\partial r} - \frac{\partial}{\partial r}\langle \rho V_z^2 \rangle - \frac{\langle \rho V_\phi^2 \rangle}{r} = -\langle \rho \frac{\partial \Phi}{\partial r} \rangle + \langle \sigma V_r \rangle. \quad (84)$$

Note that the $\partial/\partial\phi$ and $\partial/\partial z$-terms have vanished identically, the former because of the assumed periodicity and the latter because the variables ρ and V_r are presumed zero above and below the galactic disk. This is the fundamental integral equation used in section 2.3 in the main body of the paper.

We make the following top-hat definitions:

$$\langle \rho V_\phi^2 \rangle = \langle \rho \rangle V_{\phi th}^2, \quad (85)$$

$$\langle \rho V_r^2 \rangle = \langle \rho \rangle V_{rth}^2, \quad (86)$$

$$\langle \rho V_z^2 \rangle = \langle \rho \rangle V_{zth}^2, \quad (87)$$

$$\langle \rho \frac{\partial \Phi}{\partial r} \rangle = \langle \rho \rangle \frac{d\Phi_{th}}{dr}. \quad (88)$$

Now let's consider what happens if we include the result at the end of Section A.2. First let's examine the second term on the left-hand-side of equation 84; i.e., if approximately, $\langle r\rho V_r^2 \rangle \approx \langle r\rho V_r \rangle V_{rth} \approx \langle r\rho \rangle V_{rth}^2$, then we can write:

$$\begin{aligned} \frac{1}{r}\frac{\partial}{\partial r}\left(r\langle \rho V_r^2 \rangle\right) &\approx \frac{1}{r}\frac{\partial}{\partial r}\left(r\langle \rho V_r \rangle V_{rth}\right) \\ &\approx \frac{V_{rth}}{r}\frac{d}{dr}\left(r\langle \rho V_r \rangle\right) + \langle \rho V_r \rangle \frac{d}{dr} V_{rth} \\ &\approx V_{rth}\langle \sigma \rangle + \frac{\sigma_L}{r}\frac{d}{dr} V_{rth}, \end{aligned} \quad (89)$$

where we have substituted using equations 73 and 74.

If we further assume that $\langle \sigma V_r \rangle \approx \langle \sigma \rangle V_{rth}$, substitution into equation 89 yields:

$$\frac{\sigma_L}{r} \frac{d}{dr} V_{rth} - \frac{d}{dr} \langle \rho V_z^2 \rangle - \frac{\langle \rho V_\phi^2 \rangle}{r} = -\langle \rho \frac{\partial \Phi}{\partial r} \rangle. \tag{90}$$

Note that we already assumed statistically stationary for the continuity relation so we drop the time derivative here as well.

Substituting the top-hat definitions into equation 90 and dividing by $\langle \rho \rangle$ and rearranging yields:

$$\begin{aligned} \frac{d\Phi_{th}}{dr} &= \frac{V_{\phi th}^2}{r} - \frac{1}{\langle \rho \rangle} \left\{ \frac{\sigma_L}{r} \frac{dV_{rth}}{dr} + \frac{d}{dr} \left(\langle \rho \rangle V_{zth}^2 \right) \right\} \\ &= \frac{V_{\phi th}^2}{r} - \frac{dV_{zth}^2}{dr} - V_{zth}^2 \frac{d}{dr} \ln \langle \rho \rangle - \left\{ \frac{\sigma_L}{r \langle \rho \rangle} \frac{dV_{rth}}{dr} \right\}. \end{aligned} \tag{91}$$

Note that we still have the same density problem with the $\ln \langle \rho \rangle$ term if $\langle \rho \rangle \propto \exp -r/R$. But $V_z^2 << V_r^2$ (and away form the center $V_r^2 << V_\phi^2$ as well), so this term is probably negligible, even with an exponential density. A power law density creates no problems at all.

A.5 Angular momentum

The total angular momentum in an isolated galaxy is given by:

$$\begin{aligned} I_g &= \int_0^\infty dr\, r \int_0^{2\pi} d\phi \int_{-\infty}^\infty dz\, \rho(\vec{r}) \left[\vec{r} \times \vec{V} \right] \\ &= \int_0^\infty dr \int_0^{2\pi} d\phi \int_{-\infty}^\infty dz \left[r^2\, \rho(r, \phi, z)\, V_\phi(r, \phi, z) \right] \\ &= 2\pi \int_0^\infty dr\, r^2 \langle \rho(r) V_\phi(r) \rangle. \end{aligned} \tag{92}$$

This clearly implies that I_g can be finite only if $r^2 \langle \rho(r) V_\phi(r)$ is integrable. We can approximate the density velocity product using $\langle \rho(r) \rangle$ and our tophat velocity, $V_{\phi th}(r)$ as follows:

$$\begin{aligned} I_g &= 2\pi \int_0^\infty dr\, r^2 \langle \rho(r) V_\phi(r) \rangle \\ &\approx 2\pi \int_0^\infty dr \left[r^2 \langle \rho(r) \rangle V_{\phi th}(r) \right]. \end{aligned} \tag{93}$$

This is integrable only if $\langle\rho(r)\rangle\, V_{\phi th} \to 0$ faster than $1/r^3$. So if $V_{\phi th}(r) \to$ *constant* as $r \to \infty$, then we must have $\langle\rho(r)\rangle \to 0$ faster than $1/r^3$ to make the angular momentum integral finite. If $V_{\phi th}$ itself drops (as in the Milky Way) because the galaxy is flaring out, then powers of less than $1/r^3$ are acceptable. In fact, if powers less than $1/r^3$ are observed, it could be a clue that the galaxy is flaring out.

A.6 Gauss' gravitational law

Since the velocities are small compared to the speed of light, Gauss gravitational law applies. In cylindrical polar coordinates it is given by:

$$\left[\frac{1}{r}\frac{\partial}{\partial r}r\frac{\partial}{\partial r} + \frac{1}{r^2}\frac{\partial^2}{\partial\phi^2} + \frac{\partial^2}{\partial z^2}\right]\Phi(r,\phi,z) = 4\pi\, G\,\rho(r,\phi,z). \tag{94}$$

where G is the universal gravitational constant. Like the momentum equation above, we deal with the averages of this equation in the main body of the text.

We integrate this over z and average over ϕ to obtain:

$$\begin{aligned}&\langle\left[\frac{1}{r}\frac{\partial}{\partial r}r\frac{\partial}{\partial r} + \frac{1}{r^2}\frac{\partial^2}{\partial\phi^2} + \frac{\partial^2}{\partial z^2}\right]\Phi(r,\phi,z)\rangle = \\ &\frac{1}{r}\frac{d}{dr}\left(r\langle\frac{d}{dr}\Phi\rangle\right) + \left\{\frac{1}{2\pi r^2}\int_{-\infty}^{\infty}dz\left(\frac{\partial\Phi}{\partial\phi}\Big|_o^{2\pi}\right)\right\} + \left\{\frac{1}{2\pi}\int_0^{2\pi}d\phi\left(\frac{\partial\Phi}{\partial z}\Big|_{-\infty}^{\infty}\right)\right\} \\ &= 4\pi\, G\,\langle\rho(r)\rangle.\end{aligned} \tag{95}$$

But $\partial\Phi/\partial\phi|_o^{2\pi} = \partial\Phi/\partial\phi|_{2\pi} - \partial\Phi/\partial\phi|_o = 0$ since we have assumed periodic and smooth. Also:

$$\frac{\partial\Phi}{\partial z}\Big|_{-\infty}^{\infty} = \frac{\partial\Phi}{\partial z}\Big|_{\infty} - \frac{\partial\Phi}{\partial z}\Big|_{-\infty}. \tag{96}$$

We assume $\partial\Phi/\partial z$ vanishes as $|z| \to \infty$, since to not vanish would imply a finite gravitaational force at infinte distance. For a galaxy of finite extent, a finite force at infinity in any direction would surely be unphysical. Appendix B considers an alternative approach to the same conclusion using classical Green's function analysis.

Thus equation 95 reduces to:

$$\frac{1}{r}\frac{d}{dr}\left(r\langle\frac{d}{dr}\Phi\rangle\right) = 4\pi\, G\,\langle\rho(r)\rangle. \tag{97}$$

Appendix B shows several alternative ways to derive this same result using classicaal Fourier and Bessel analysis.

Now we can use this to define our 'momentum thickness', $z_m(r)$, by:

$$z_m(r)\,\frac{d\Phi_{th}(r)}{dr} = \frac{1}{2\pi}\int_0^{2\pi}d\phi\int_{-\infty}^{\infty}dz\,\frac{\partial\Phi(r,\phi,z)}{\partial r}. \tag{98}$$

Note that $d\Phi_{th}(r)/dr$ has already been defined in equation 88. So our gravitational law reduces to:

$$\frac{1}{r}\frac{d}{dr}\left[r\left(z_m\frac{d}{dr}\Phi_{th}\right)\right] = 4\pi\, G\,\langle\rho(r)\rangle. \tag{99}$$

Substituting from equation 91 yields:

$$\frac{1}{r}\frac{d}{dr}\left[r\left(z_m\left\{\frac{V_{\phi th}^2}{r} - \frac{dV_{zth}^2}{dr} - V_{zth}^2\frac{d}{dr}\ln\langle\rho\rangle - \left\{\frac{\sigma_L}{r\langle\rho\rangle}\frac{dV_{rth}}{dr}\right\}\right\}\right)\right] = 4\pi\, G\,\langle\rho(r)\rangle. \tag{100}$$

Or clearing the r terms:

$$\frac{1}{r}\frac{d}{dr}\left(z_m\left[V_{\phi th}^2 - r\frac{dV_{zth}^2}{dr} - rV_{zth}^2\frac{d}{dr}\ln\langle\rho\rangle - \frac{\sigma_L}{\langle\rho\rangle}\frac{dV_{rth}}{dr}\right]\right) = 4\pi\, G\,\langle\rho(r)\rangle. \tag{101}$$

Note that $\sigma_L(r)$ is given by 73; so reversing the sides:

$$\sigma_L = r\langle\rho(r)V_r(r)\rangle \approx r\langle\rho(r)\rangle V_{rth}(r). \tag{102}$$

So if we know $\langle\rho\rangle$ and V_{rth}, we can determine σ_L.

Alternatively we can substitute equation 102 into equation 101 to obtain:

$$\frac{1}{r}\frac{d}{dr}\left(z_m\left[V_{\phi th}^2 - \frac{1}{2}r\frac{dV_{rth}^2}{dr} - r\frac{dV_{zth}^2}{dr} - rV_{zth}^2\frac{d}{dr}\ln\langle\rho\rangle\right]\right) = 4\pi\, G\,\langle\rho(r)\rangle. \tag{103}$$

This form is particularly nice since it includes the source terms implicitly in the dV_{rth}^2/dr-term. Note that if $dV_{rth}^2/dr \leq 0$, $dV_{zth}^2/dr \leq 0$ and $d\langle\rho\rangle/dr < 0$ for large r, these extra terms act to decrease the product $z_m V_{\phi th}^2$ for any given density distribution on the right-hand-side.

B Alternative derivation of momentum and gravitational law integrals

This appendix shows an alternative derivation of the results of Sections 2.3 and 2.4 in the main body of the text using standard Fourier and Bessel function analyses. The results are the same, but instructive none-the-less.

B.1 Fourier decomposition of gravitational potential and density

We begin by representing the three-dimensional gravitational potential as a Fourier series in ϕ and a Fourier transform over z: i.e.,

$$\Phi(r,\phi,z) = \sum_{m=-\infty}^{\infty}\int_{-\infty}^{\infty} dk\,\hat{\Phi}(r,k,m)\,e^{+i\,(m\,\phi+\,k\,z)}, \tag{104}$$

$$\rho(r,\phi,z) = \sum_{m=-\infty}^{\infty}\int_{-\infty}^{\infty} dk\,\hat{\rho}(r,k,m)\,e^{+i\,(m\,\phi+k\,z)}, \tag{105}$$

where $\hat{\Phi}(r,m,k)$ and $\hat{\rho}(r,m,k)$ are the corresponding Fourier series and Fourier transform coefficients defined as:

$$\hat{\Phi}(r,m,k) = \left[\frac{1}{2\pi}\right]^2\int_0^{2\pi} d\phi\int_{-\infty}^{\infty} dz\,\Phi(r,\phi,z)\,e^{-i\,(m\,\phi+\,k\,z)}, \tag{106}$$

$$\hat{\rho}(r,m,k) = \left[\frac{1}{2\pi}\right]^2\int_0^{2\pi} d\phi\int_{-\infty}^{\infty} dz\,\rho(r,\phi,z)\,e^{-i\,(m\,\phi+k\,z)}. \tag{107}$$

We note that the transforms of the derivatives of $\Phi(r,\phi,z)$ are given by:

$$FT\{\partial\Phi(r,\phi,z)/\partial z\} = -i\,k\,\hat{\Phi}(r,k,m), \tag{108}$$

$$FT\{\partial\Phi(r,\phi,z)/\partial\phi\} = -i\,m\,\hat{\Phi}(r,k,m). \tag{109}$$

B.2 From Poisson (Gauss' Law) to Bessel

Transforming both sides of our Poisson equation yields:

$$\left[\frac{1}{r}\frac{\partial}{\partial r}\left(r\frac{d}{dr}\right) - (\frac{m^2}{r^2}+k^2)\right]\hat{\Phi}(r,m,k) \;=\; 4\pi\,G\,\hat{\rho}(r,m,k). \tag{110}$$

This is a form of Bessel's equation that has traditionally been solved using Green's functions. For three-dimensional cylindrical coordinates this is not trivial (c. f. [37]). We will show a solution solved this way in Section B.4. But given that our sole interest is in the results averaged over ϕ and integrated over z there is an almost trivial way to get to the desired solution. We present this first, then show both solutions are the same.

B.3 The fast way using properties of Fourier methods

Note what happens to the Fourier transformed gravitational potential and density fields if we set $m = 0$ and $k = 0$ in equations 106 and 107 and multiply by 2π; i.e.,

$$2\pi\,\hat{\Phi}(r,0,0) \;= 2\pi\,\hat{\Phi}(r, m=0, k=0) \quad = \quad \left[\frac{1}{2\pi}\right] \int_{-\infty}^{\infty} dz\,\Phi(r,\phi,z), \quad (111)$$

$$2\pi\,\hat{\rho}(r,0,0) = 2\pi\,\hat{\rho}(r, m=0, k=0) \quad = \quad \left[\frac{1}{2\pi}\right] \int_{-\infty}^{\infty} dz\,\rho(r,\phi,z), \quad (112)$$

since the exponentials just reduce to 1. The integrals on the right-hand-side are **exactly** the un-transformed quantities integrated over z and averaged over ϕ we seek, $\langle\Phi(r)\rangle$ and $\langle\rho(r)\rangle$; namely,

$$\langle\Phi(r)\rangle \quad = \quad \left[\frac{1}{2\pi}\right] \int_{-\infty}^{\infty} dz\,\Phi(r,\phi,z) = [2\pi]\;\hat{\Phi}(r,0,0), \quad (113)$$

$$\langle\rho(r)\rangle \quad = \quad \left[\frac{1}{2\pi}\right] \int_{-\infty}^{\infty} dz\,\rho(r,\phi,z) = [2\pi]\;\hat{\rho}(r,0,0). \quad (114)$$

Similarly, the average over ϕ and integral over z of the potential gradient, $\langle\partial\Phi(r)\rangle$ is given by:

$$\langle\frac{\partial\langle\Phi(r,\phi,z)}{\partial r}\rangle = 2\,\pi\,\frac{\partial\hat{\Phi}(r,0,0)}{\partial r}. \quad (115)$$

We can use these to rewrite our Bessel equation. Setting $m = 0$ and $k = 0$ in equation 110 yields:

$$\frac{1}{r}\frac{d}{dr}\left(r\frac{\partial\hat{\Phi}(r,0,0)}{\partial r}\right) \quad = \quad 4\pi G\hat{\rho}(r,0,0). \quad (116)$$

Or equivalently using equations 114 and 115:

$$\frac{1}{r}\frac{d}{dr}\left(r\;\langle\frac{\partial\Phi(r)}{\partial r}\rangle\right) = 4\pi G\,\langle\rho(r)\rangle. \quad (117)$$

Thus we have a direct expression relating the spatially averaged gravitational potential, $\langle\partial\Phi(r)/\partial r\rangle$, to the spatially-averaged density, $\langle\rho(r)\rangle$. This can be integrated from 0 to r to obtain:

$$r\;\langle\frac{\partial\Phi(r)}{\partial r}\rangle = 4\pi G\int_0^r \langle\rho(r')\rangle\,r'\,dr'. \quad (118)$$

This is exactly equation 25 which we obtained in the main body of text by averaging over ϕ and integrating over z and appling the boundary condition that $\partial\Phi(r,\phi,z)/\partial z$ vanishes in the limit as $|z| \to 0$.

B.4 Complete solution using modified Bessel functions

The lecture notes of Fitzpatric [37] present an elegant and interesting derivation of the complete solution to equation 110 for homogeneous boundary conditions. First he derives a Green's function in cylindrical coordinates using modified Bessel functions, $I_m(kr)$ and $K_m(kr)$. What makes this particularly interesting is that I_m blows up as $k\,r \to \infty$ while the second blows up as $k\,r \to 0$. So the solution is spliced together in two parts by multiplying them together. The final result is:

$$\hat{\Phi}(r,m,k) = [4\pi G]\left\{K_m(k\,r)\int_0^r \hat{\rho}(r',m,k))I_m(k\,r')\,r'dr' + I_m(k\,r)\int_r^\infty \hat{\rho}(r',m,k)\,K_m(k\,r')r'dr'\right\}. \tag{119}$$

Now we can use the same Fourier transform 'trick' we used in Section B.3 above to obtain the integrated density and gravitation profiles directly by setting m and taking the limit as $k \to 0$; i.e.,

$$\hat{\Phi}(r,0,0) = [4\pi G]\lim_{k\to 0}\left\{K_0(k\,r)\int_0^r \hat{\rho}(r',0,0))I_0(k\,r')\,r'dr' + I_0(k\,r)\int_r^\infty \hat{\rho}(r',0,0)\,K_0(k\,r')r'dr'\right\}. \tag{120}$$

The Bessel functions have the following properties in the limit as their arguments go to zero:

$$I_0(x) \;\to\; 1, \tag{121}$$

$$I_0'(x) \;=\; \frac{1}{2}\left[I_{-1} + I_{+1}\right] = I_1 = \frac{x}{2}, \tag{122}$$

$$K_0(x) \;\to\; -\gamma - \ln(x/2), \tag{123}$$

$$K_0'(x) \;\to\; -1/x, \tag{124}$$

where γ is Euler's constant (v. [1, 42]).

It is straightforward to show by integration by parts and differentiation with respect to r of equation 120 that this yields exactly the results of equations 116 to 118 above. Note that it is the differentiation of the $\ln(k\,r)$-term (from $K_0(k\,r)$ that produces the $1/r$-dependence necessary to cancel the $1/r$ multiplying the velocity-squared. And this in turn produces the observed asymptotic velocities which do not die off like the planetary results.

Alternatively equation 117 can be differentiated directly with respect to r to yield:

$$\begin{aligned}
\frac{\partial\hat{\Phi}(r,0,0)}{\partial r} &= [4\pi G]\lim_{k\to 0}\left\{k\,K_0'(k\,r)\int_0^r \hat{\rho}(r',0,0))I_0(k\,r')\,r'dr'\right. \\
&\qquad \left. - k\,I_0'(k\,r)\int_r^\infty \hat{\rho}(r',0,0)\,K_0(k\,r')r'dr'\right\} \\
&= [4\pi G]\lim_{k\to 0}\left\{k\,(\frac{1}{k\,r})\int_0^r \hat{\rho}(r',0,0))\,1\,r'dr'\right. \\
&\qquad \left. - k\,(\frac{k\,r}{2})\int_r^\infty \hat{\rho}(r',0,0)\;[-\ln(\gamma\,k\,r'/2)]\,r'dr'\right\} \\
&= [4\pi G]\left\{\frac{1}{r}\int_0^r \hat{\rho}(r',0,0))\,r'dr'\right\}. \qquad (125)
\end{aligned}$$

If we multiply both sides by 2π and use the Fourier transform limit trick, we recover exactly equation 25.

B.5 Combining Bessel and the momentum equations

We know from the main body of the text and Appendix 1.2 that our momentum integral equation integrated over z and averaged over ϕ reduces to:

$$\langle V_\phi^2\rangle - \frac{r}{2}\frac{d}{dr}\langle V_r^2\rangle = r\,\langle\frac{d\Phi(r)}{dr}\rangle. \qquad (126)$$

We note that all dependent variables are fields, so we can substitute from one equation to another. Substituting for the spatially-averaged potential gradient from the momentum integral of equation 126 into equation 117 yields immediately our original result in the main body of the text; namely:

$$\frac{1}{r}\frac{d}{dr}\left(\langle V_\phi^2\rangle - \frac{r}{2}\frac{d}{dr}\langle V_r^2\rangle\right) = 4\pi G\langle\rho(r)\rangle. \qquad (127)$$

Thus by using Fourier analysis in a clever way we have found an alternative route to the same result we obtained in the main body of the text by simply integrating the equations directly.

B.6 The hazards of solving the hard way

A much more complicated approach is to actually solve equation 110 to obtain $\hat{\Phi}(r,m,k)$ as we did in Section B.4 above for an *assumed three-dimensional density* distribution.[4] Then inverting the Fourier transform and Fourier series coefficients using equation 104 by integrating over all k and performing the infinite sum over m to get the gravitational potential in physical variables: i.e.,

[4]Note that the three-dimensional density is usually *assumed*, since almost always only the two-dimensional one, $\langle\rho(r)\rangle$, can be measured.

$$\Phi(r,\phi,z) = \sum_{m=-\infty}^{\infty} \int_{-\infty}^{\infty} dk\, e^{+i[m\,\phi + k\,z]}\, \hat{\Phi}(r,\phi,z). \tag{128}$$

Then differentiating to find $\partial\Phi(r,\phi,z)/\partial r$.

Some papers (e.g. Eilers et al.[11]) take the $\partial\Phi(r,\phi,z)/\partial r$ so computed (or by numerical equivalent), evaluate it along $z = 0$ and set this equal to V_ϕ^2/r (or the circular velocity equivalent, V_c^2/r, computed from Jeans equation); i.e.,

$$\frac{V_\phi^2}{r} \text{ or } \frac{V_c^2}{r} = \left.\frac{\partial\Phi}{\partial r}\right|_{z=0}. \tag{129}$$

But as noted above, this requires summing over all m values and integrating over all k from $-\infty$ to ∞. In principle, this should be straight-forward. But given the results cited in the various papers (which seldom explain what they actually did), apparently not. The reason we suspect is most likely due to a mishandling of the logarithmic singularity, from $K_0(k\,r)$ at the origin in equation 120. Singularities at the origin in Fourier space always appear at large values in physical space. By contrast, our solution can be obtained by simply setting $k = 0$ and $m = 0$ in the Bessel solutions above.

So what exactly have others done? Most early contributors (e. g. Oort [33], Zwicky [45], Ruben et al. [35] avoided solving the Gauss' Law equation entirely, clearly expecting galaxies to behave as a planetary system. Others more recently (e. g. , Eilers et al. [11], McGaugh et al. [31]) have tried to actually solve the equation as we have done above, either analytically or numerically. All seem to show the opposite of what we derive here: all their computed potential gradients decrease with increasing radius, similar to the planetary results. It is not hard to imagine why – especially given the logarithmic singularity at $k\,r = 0$. In fact as we discovered ourselves, if not handled properly it leads to the erroneous conclusion that the gravitational potential dies off faster than $1/r$ with distance.

B.7 Summary of this appendix

Luckily our result here and in the main body of the text appears to be true and quite independent of the Bessel solutions above using I_o and K_o, and even the Green's function as derived in [37]. In light of our observation above about the behavior of the particular solution involving Bessel functions when inverse transforming, this is good. Clearly our solution here depends only on the Fourier series and transform representations. The former always exist for periodic processes (which we have by assumption), and the Fourier transforms almost always exist, at least in the sense of generalized functions (c.f. [29, 28]). Surely they exist for any physical z-profile.

Our solution in the main body of the text depended only on $\partial\Phi/\partial z$ vanishing in the limit as $|z| \to \infty$ (a Dirichlet boundary condition and only in one direction). Note that most (maybe all) papers, past and present, say little to nothing about how they solved the Poisson equation. Nor none, as best we can

tell, worked with integrated equations. Given that the measurements of density in particular were always integrated across the galaxy thickness, this seems a major oversight.

C An equilibrium similarity solution for galaxies

We seek a similarity solution of the equations of Section 83 of the form:

$$\begin{aligned}
\rho(r,z,\phi) &= \rho_s(r,\phi)\, f_\rho(\eta), && (130)\\
V_\phi(r,z,\phi) &= V_{s\phi}(r,\phi)\, F_\phi(\eta), && (131)\\
V_r(r,z,\phi) &= V_{sr}(r,\phi)\, F_r(\eta), && (132)\\
V_z(r,z,\phi) &= V_{sz}(r,\phi)\, F_z(\eta), && (133)\\
\Phi(r,z,\phi) &= \Phi_s(r,\phi)\, g(\eta), && (134)
\end{aligned}$$

where η is defined to be:

$$\eta = \frac{z}{\delta(r)}. \qquad (135)$$

The functions with subscript 's' are 'scale functions' which depend only on r and ϕ, and the functions multiplying them have the scaled z-dependence. Note that we have suppressed any time dependence, at least for now. Also we do not need to independently consider σ since it is simply related to V_r through the continuity equation.

It is important to also note that at this point we are merely transforming the equations, and making no assumptions about them. If there are no solutions of the form we seek, we won't find any. But if there is such a solution we hope that $\delta(r)$ can be identified with our momentum thickness, $z_m(r)$.

C.1 Similarity of the r-momentum equation

We consider the terms in the statistically stationary radial moment equation 83. Note that we could have kept the $\partial/\partial t$-term, but for now restrict ourselves to galaxies in equilibrium. Substituting our similarity transformations into the terms one-by-one yields the following:

$$\frac{1}{r}\frac{\partial(r\,\rho\,V_r^2)}{\partial r} = \frac{\rho\,V_r^2}{r} + \frac{\partial(\rho\,V_r^2)}{\partial r}, \tag{136}$$

$$= \left[\frac{\rho_s\,V_{sr}^2}{r} + \frac{\partial}{\partial r}\left\{\rho_s V_{sr}^2\right\}\right]\left(f_\rho\,F_r^2\right) - \left[\rho_s\,V_{sr}^2\right]\left[\frac{1}{\delta}\frac{d\delta}{dr}\right]\,\eta\frac{d}{d\eta}\left(f_\rho\,F_r^2\right),$$

$$\frac{1}{r}\frac{\partial(\rho V_\phi V_r)}{\partial\phi} = \left[\frac{1}{r}\,\frac{\partial}{\partial\phi}\left\{\rho_s\,V_{s\phi}\,V_{sr}\right\}\right]\,\left(f_\rho\,F_\phi F_r\right), \tag{137}$$

$$\frac{\partial(\rho V_r V_z)}{\partial z} = \left[\frac{\rho_s\,V_{sr}\,V_{sz}}{\delta}\right]\,\frac{d}{d\eta}(f_\rho\,F_r\,F_z), \tag{138}$$

$$\rho\frac{V_\phi^2}{r} = \left[\frac{\rho_s\,V_{s\phi}^2}{r}\right]\left(f_\rho\,F_\phi^2\right), \tag{139}$$

$$\rho\,\frac{\partial\overline{\Phi}}{\partial r} = \left[\rho_s\frac{\partial\Phi_s}{\partial r}\right](f_\rho g_s) - [\rho_s\Phi_s]\left[\frac{1}{\delta}\frac{d\delta}{dr}\right]\,\left(\eta f_\rho\,\frac{dg}{d\eta}\right) \tag{140}$$

$$= \left[\frac{\rho_s\Phi_s}{r}\right]\left\{\left[\frac{\partial\ln\Phi_s}{\partial\ln r}\right](f_\rho g) - \left[\frac{d\ln\delta}{d\ln r}\right]\,\left(\eta f_\rho\,\frac{dg}{d\eta}\right)\right\}. \tag{141}$$

Note that on the right-hand-side we have grouped all the r,ϕ-dependent terms in square brackets, and the η and ϕ-dependent terms in parentheses. We shall follow this convention throughout, unless parentheses are necessary inside the square brackets for clarity.

These square-bracketed terms all have the same r-dependence if:

$$\left[\frac{\rho_s\,V_{sr}^2}{r}\right] + \left[\frac{\partial}{\partial r}\left\{\rho_s V_{sr}^2\right\}\right] \propto \left[\frac{\rho_s\,V_{sr}^2}{\delta}\frac{d\delta}{dr}\right] \propto \left[\frac{1}{r}\,\frac{\partial}{\partial\phi}\left\{\rho_s\,V_{s\phi}\,V_{sr}\right\}\right]$$
$$\propto \left[\frac{\rho_s\,V_{sr}\,V_{sz}}{\delta}\right] \propto \left[\frac{\rho_s\,V_{s\phi}^2}{r}\right] \propto \left[\rho_s\frac{\partial\Phi_s}{\partial r}\right] \propto [\rho_s\Phi_s]\left[\frac{1}{\delta}\frac{d\delta}{dr}\right]. \tag{142}$$

We have deliberately grouped the $r-\phi$-dependent terms together if they multiply the same η-dependent terms since the r,ϕ-terms may cancel each other out.

The proportionality between all the quantities in equation 142 can be satisfied only if:

$$\left[\frac{r}{\delta}\frac{d\delta}{dr}\right] = \left[\frac{d\ln\delta}{d\ln r}\right] = const, \tag{143}$$

$$\left[\frac{\partial}{\partial r}(r\,\rho_s V_{sr}^2)\right] \propto V_{s\phi}^2(r,\phi), \tag{144}$$

$$\frac{V_{s\phi}^2(r,\phi)}{V_{sr}^2(r,\phi)} \propto \left[\frac{d\,\ln\delta(r)}{d\ln r}\right] = const, \tag{145}$$

$$\frac{V_{sz}(r,\phi)}{V_{sr}(r,\phi)} \propto \frac{d\delta(r)}{dr}, \tag{146}$$

$$\frac{V_{s\phi}^2(r,\phi)}{\Phi_s(r,\phi)} \propto \left[\frac{d\ln\delta}{d\ln r}\right] = const, \tag{147}$$

$$\left[\frac{\partial\ln\Phi_s(r,\phi)}{\partial\ln r}\right] \propto \left[\frac{V_{s\phi}^2}{V_{sr}^2}\right] = const. \tag{148}$$

We have kept squared velocities together since we intend to average their squares later. From the last equation, equation 144 we can see that the galaxy similarity solution is a true logarithmic spiral, since the ratio of V_{sr} to $V_{s\phi}$ is constant. We note for future use, equation 145, since this is the term we have identified as problematical in the classical approach (e.g. [11]). Since its r-dependence is directly proportional to $V_{s\phi}^2$, clearly it should not be. So if it is, something is wrong. The term involving the partial derivative with respect to ϕ is very interesting, but we defer discussion of it to below.

C.2 Similarity of the continuity equation

Now we consider the continuity equation given by equation 69. Ignoring the time term and treating these as averages yields for the individual terms:

$$\frac{1}{r}\frac{\partial}{\partial r}(r\rho V_r) = \left[\frac{\rho_s V_{sr}}{r} + \frac{\partial}{\partial r}\left\{\rho_s V_{sr}\right\}\right](f_\rho F_r) - \left[\frac{\rho_s V_{sr}}{\delta}\frac{d\delta}{dr}\right]\eta\frac{d}{d\eta}(f_\rho F_r), \tag{149}$$

$$\frac{1}{r}\frac{\partial}{\partial\phi}(\rho V_\phi) = \left[\frac{1}{r}\frac{\partial}{\partial\phi}\left\{\rho_s V_{s\phi}\right\}\right] f_\rho F_\phi, \tag{150}$$

$$\frac{\partial}{\partial z}(\rho V_z) = \left[\frac{\rho_s V_{sz}}{\delta}\right]\frac{d}{d\eta}(f_\rho F_z). \tag{151}$$

Note that the time derivative term could also have been included, as well as the source term. The time scale would have to be chosen to satisfy the additional term.

Full equilibrium similarity requires that any non-zero terms have the same r and ϕ-dependence; i.e.,

$$\left[\frac{\rho_s V_{sr}}{r}\right] \propto \left[\frac{\partial}{\partial r}\left\{\rho_s V_{sr}\right\}\right] \propto \left[\frac{\rho_s V_{sr}}{\delta}\frac{d\delta}{dr}\right] \propto \left[\frac{1}{r}\frac{\partial}{\partial\phi}\left\{\rho_s V_\phi\right\}\right] \propto \left[\frac{\rho_s V_{sz}}{\delta}\right]. \tag{152}$$

The second and last terms are exactly equation 146, and show clearly how the entrainment and growth rate of the disk with r are related. The $\partial/\partial\phi$-term we will discuss in detail later in Section C.5 below.

The first two terms on the left-hand side resemble equation 144, but have a factor V_{sr} instead of V_{sr}^2; i.e.,

$$\left[\frac{\partial}{\partial \ln r}(\ln r\, \rho_s V_{sr})\right] \propto \left[\frac{d \ln \delta}{d \ln r}\right] = constant. \tag{153}$$

It is straight-forward to show that both can be true:

$$\begin{aligned}
\left[\frac{\partial}{\partial \ln r}(\ln r\, \rho_s V_{sr})\right] &= \frac{\partial}{\partial \ln r}\left[\ln r + \ln \rho_s + \ln V_{sr}\right] \propto \left[\frac{d \ln \delta}{d \ln r}\right], \\
\left[\frac{\partial}{\partial \ln r}(\ln r\, \rho_s V_{sr}^2)\right] &= \frac{\partial}{\partial \ln r}\left[\ln r + \ln \rho_s + 2\, \ln V_{sr}\right] \propto \left[\frac{d \ln \delta}{d \ln r}\right].
\end{aligned}$$

Subtraction of the upper from the lower yields:

$$2\, \frac{\partial}{\partial \ln r} \ln V_{rs} \propto \frac{\partial}{\partial \ln r} \ln V_{rs}, \tag{154}$$

which is surely true.

Finally we note the interesting relation between the ϕ-derivative of $V_{s\phi}$ and V_z; i.e.,

$$\left[\frac{1}{r}\frac{\partial}{\partial \phi}\left\{\rho_s V_\phi\right\}\right] \propto \left[\frac{\rho_s V_{sz}}{\delta}\right]. \tag{155}$$

This clearly shows that the Fourier component of any entrainment velocity, $V_{sz}(r, \phi)$ must be ninety degrees out of out of phase with the azimuthal velocity, $V_{s\phi}(r, \phi)$. **So there must be rotation around any spiral if the galaxy thickness grows.**

C.3 Similarity of Gauss' gravitational law

We start with Gauss' gravitational law in cylindrical coordinates:

$$\left[\frac{1}{r}\frac{\partial}{\partial r}\left(r\frac{\partial}{\partial r}\right) + \frac{1}{r^2}\frac{\partial^2}{\partial \phi^2} + \frac{\partial^2}{\partial z^2}\right] \Phi(r, \phi, z) = 4\pi\, G\, \rho(r, \phi, z). \tag{156}$$

Transforming the first term on the left-hand-side yields:

$$
\begin{aligned}
\frac{1}{r}\frac{\partial}{\partial r}\left(r\frac{\partial}{\partial r}\right)\Phi(r,\phi,z) &= \frac{1}{r}\frac{\partial}{\partial r}r\left\{\left[\frac{\partial\Phi_s}{\partial r}\right]g(\eta)-\left[\frac{\Phi_s}{\delta}\frac{d\delta}{dr}\right]\eta\frac{dg}{d\eta}\right\} \\
&= \frac{1}{r}\frac{\partial}{\partial r}\left\{\Phi_s\left[\frac{\partial\ln\Phi_s}{\partial\ln r}\right]g(\eta)-\left[\Phi_s\frac{d\ln\delta}{d\ln r}\right]\eta\frac{dg}{d\eta}\right\} \qquad (157)\\
&= \left[\frac{\partial^2\Phi_s(r,\phi)}{\partial r^2}+\frac{1}{r}\frac{\partial\Phi_s(r,\phi)}{\partial r}\right](g(\eta)) \\
&\quad -\Phi_s(r,\phi)\frac{\partial}{\partial r}\left\{\left[\frac{1}{\delta(r)}\frac{d\delta}{dr}\right]\left(\eta\frac{\partial g}{\partial\eta}\right)\right\} \\
&\quad -\left[\frac{\Phi_s}{r}+\frac{\partial\Phi_s}{\partial r}\right]\left[\frac{1}{\delta}\frac{d\delta}{dr}\right]\left(\eta\frac{dg}{d\eta}\right) \\
&= \left[\frac{\partial^2\Phi_s(r,\phi)}{\partial r^2}+\frac{1}{r}\frac{\partial\Phi_s(r,\phi)}{\partial r}\right](g(\eta)) \qquad (158)\\
&\quad -\Phi_s(r,\phi)\left\{\left[\frac{d^2\ln\delta}{dr^2}\right]\left(\eta\frac{\partial g}{\partial\eta}\right)+\left[\frac{1}{\delta}\frac{d\delta}{dr}\right]^2\left(\eta\frac{d}{d\eta}\left(\eta\frac{dg}{d\eta}\right)\right)\right\} \\
&\quad -\left[\frac{\Phi_s}{r}+\frac{\partial\Phi_s}{\partial r}\right]\left[\frac{1}{\delta}\frac{d\delta}{dr}\right]\left(\eta\frac{dg}{d\eta}\right).
\end{aligned}
$$

Note that we really need only the second line, equation 157, since we are going to substitute for it using equation 142. But transforming the second and third terms on the left-hand-side of equation 156 anyway yields:

$$
\begin{aligned}
\frac{1}{r^2}\frac{\partial^2}{\partial\phi^2}\Phi(r,\phi,z) &= \left[\frac{1}{r^2}\frac{\partial^2\Phi_s}{\partial\phi^2}\right](g)\,, \qquad (159)\\
\frac{\partial^2}{\partial z^2}\Phi(r,\phi,z) &= \left[\frac{\Phi_s}{\delta^2}\right](\frac{d^2g}{d\eta^2}). \qquad (160)
\end{aligned}
$$

As before, for an equilibrium similarity solution, all the non-zero square bracketed terms must have the same r-dependence; i.e.,

$$
\begin{aligned}
&\left[\frac{\partial^2\Phi_s(r,\phi)}{\partial r^2}+\frac{1}{r}\frac{\partial\Phi_s(r,\phi)}{\partial r}\right]=\left[\frac{1}{r}\frac{\partial}{\partial r}\left(r\frac{\partial\Phi_s}{\partial r}\right)\right] \\
&\propto \frac{\Phi_s(r,\phi)}{r^2}\left[\frac{d\ln\delta}{d\ln r}\right]\propto\frac{\Phi_s}{r^2}\left[\frac{d\ln\delta}{d\ln r}\right]^2\propto\frac{\Phi_s}{r^2}\left[\frac{d^2\ln\delta}{d\ln r^2}\right] \\
&\propto\left[\frac{1}{r^2}\frac{\partial^2\Phi_s}{\partial\phi^2}\right]\propto\left[\frac{\Phi_s}{\delta^2}\right]\propto G\left[\rho_s\right], \qquad (161)
\end{aligned}
$$

where the last term arises from the right-hand-side of equation 156.

There seems to be only one way to satisfy these three conditions:

$$
\frac{\Phi_s(r,\phi)}{r^2}\left[\frac{d\ln\delta}{d\ln r}\right]\propto\frac{\Phi_s}{r^2}\left[\frac{d\ln\delta}{d\ln r}\right]^2\propto\frac{\Phi_s}{r^2}\left[\frac{d^2\ln\delta}{d\ln r^2}\right]; \qquad (162)
$$

namely, $d\ln\delta/d\ln r = constant$. But we must also satisfy:

$$\frac{\Phi_s(r,\phi)}{r^2}\left[\frac{d\ln\delta}{d\ln r}\right] \propto \left[\frac{\Phi_s(r,\phi)}{\delta^2(r)}\right]. \tag{163}$$

We also know that $d\ln\delta/d\ln r = constant$, so there are only two possible solutions: either

$$\delta(r) \propto r; \tag{164}$$

or

$$\delta = constant. \tag{165}$$

Equation 164 implies immediately that:

$$\frac{d\ln\delta}{d\ln r} = 1 \quad \text{or} \quad 0 \tag{166}$$

So wherever this factor occurs, we can simply replace it by 1 or 0.

Note that the next to last term, Φ_s/δ^2, arises from the $\partial^2\Phi/\partial z^2$. **So if for some reason this term (or its integrals) vanish identically (say due to symmetry in the η-direction), this condition falls out of the analysis.** So it, like the condition for the constancy of the ratio of $V_{s\phi}$ to V_{sr}, could not have been deduced from only an integral analyses.

C.4 The integrated density, $\overline{\rho}$

To this point in our similarity analysis we've been dealing with the actual three-dimensional density, $\rho(r,\phi,z) = \rho_s(r,\phi)f_\rho(\eta)$. But all of the data deal with the density, $\langle\rho(r)\rangle$, which has been integrated across the disk in the z-direction AND averaged over ϕ. Now we need another density which has only been integrated over z, say $\overline{\rho}(r,\phi)$, defined by:

$$\overline{\rho}(r,\phi) = \int_{-\infty}^{\infty}\rho(r,\phi,z)dz. \tag{167}$$

Note that for now we use the overline to distinguish this density from the one averaged over ϕ and integrated over z.

Substituting for $\rho(r,\phi,z)$ yields:

$$\overline{\rho}(r,\phi) = [\rho_s(r,\phi)\,\delta(r)]\int_{-\infty}^{\infty}f_\rho(\eta)d\eta. \tag{168}$$

So the r-dependence of the scale for the integrated density will differ by a factor of $\delta(r)$ from ρ_s, and by a coefficient determined by the integral of the profile shape.

C.5 The ϕ-dependence

We can express $\rho_s(r,\phi)$ and $\Phi_s(r,\phi)$ as a Fourier series in ϕ, say:

$$\Phi_s(r,\phi) = \Sigma_{-\infty}^{\infty} e^{-i2\pi m\phi}\hat{\Phi_s}(r,m), \tag{169}$$

$$\rho_s(r,\phi) = \Sigma_{-\infty}^{\infty} e^{-i2\pi m\phi}\hat{\rho}_\rho(r,m). \tag{170}$$

For $m = 0$, the term $\partial^2\Phi_s/\partial\phi^2 = 0$ and we are left with:

$$\hat{\Phi}_s(r,0) \propto G\,\delta^2(r)\,\hat{\rho}_s(r,0). \tag{171}$$

But $\hat{\Phi}(r,0)$ and $\hat{\rho}_s(r,0)$ are just the azimuthally averaged values of Φ_s and ρ_s, say $\overline{\Phi}(r,z)$ and $\overline{\rho}(r,z)$. So the aziumthally-averaged potential and three-dimensional density are related by

$$\overline{\Phi}(r,z) \propto G\,\delta^2(r)\,\overline{\rho}(r,z). \tag{172}$$

For $m \neq 0$ the $\partial^2/\partial\phi^2$ term is in general not zero, so the last three terms of equation 161 require:

$$-(2\pi m)^2\,\frac{\hat{\Phi}_s(r,m)}{r^2} \propto \frac{\hat{\Phi}_s(r,m)}{\delta^2} \propto G\,[\hat{\rho}_s(r,m)]. \tag{173}$$

Thus if there are terms for which $m \neq 0$, then we must have

$$\delta \propto \frac{r}{2\pi m}. \tag{174}$$

Note that this condition applies ONLY for $m \neq 0$, so clearly it applies only to azimuthally asymmetric or spiral galaxies! But it suggests that the actual spreading rate of the galactic disk might be dominated by its mean or low Fourier components.

C.6 A complete similarity solution

A useful relation follows from the first line in equation 161:

$$\frac{1}{r}\frac{\partial}{\partial r}\left\{r\frac{\partial\Phi_s}{\partial r}\right\} \propto G[\rho_s]. \tag{175}$$

From equation 148 we have:

$$\frac{\partial\Phi_s}{\partial r} \propto \frac{V_{s\phi}^2}{r}. \tag{176}$$

Substitution into equation 175 yields immediately that:

$$\frac{1}{r}\frac{\partial}{\partial r}V_{s\phi}^2 \propto G[\rho_s]. \tag{177}$$

Or integrating:

$$V_{s\phi}^2(r,\phi) \propto G\int_0^r \rho_s(r',\phi)r'dr'. \tag{178}$$

From the last three terms of equation 142 by removing the common factor, ρ_s/r, we have:

$$\left[V_{s\phi}^2\right] \propto \left[r\,\frac{\partial \Phi_s}{\partial r}\right] - \left[r\,\Phi_s\right]\left[\frac{1}{\delta}\frac{d\delta}{dr}\right]. \tag{179}$$

Substituting this into equation 175 yields:

$$\frac{1}{r}\left\{\frac{\partial}{\partial r}V_\phi^2\right\} \propto G[\rho_s]. \tag{180}$$

But this is our previous result in the main body of the text, equation 32 and those that followed.

C.7 Collecting all terms using similarity relations

Now we seem to have all the pieces. So we need to return to the full equations and try to solve them, presumably by integrating over η. We have shown that indeed the conditions for an equilibrium similarity solution can be satisfied. So now we return to equation 83 to see what the final equation as a function of η only looks like. We will not use this result in this paper, so it is of academic interest only for now.

To begin, we substitute all of our similarity relations into equation 83:

$$\begin{aligned}
&\left[\frac{\rho_s\,V_{sr}^2}{r} + \frac{\partial}{\partial r}\left\{\rho_s V_{sr}^2\right\}\right]\left(f_\rho\,F_r^2\right) - \left[\rho_s\,V_{sr}^2\right]\left[\frac{1}{\delta}\frac{d\delta}{dr}\right]\,\eta\frac{d}{d\eta}\left(f_\rho\,F_r^2\right)\\
&+\left[\frac{1}{r}\,\frac{\partial}{\partial\phi}\left\{\rho_s\,V_{s\phi}\,V_{sr}\right\}\right]\,\left(f_\rho\,F_\phi F_r\right) + \left[\frac{\rho_s\,V_{sr}\,V_{sz}}{\delta}\right]\,\frac{d}{d\eta}(f_\rho\,F_r\,F_z)\\
&-\left[\frac{\rho_s\,V_{s\phi}^2}{r}\right]\left(f_\rho\,F_\phi^2\right)\\
&=-\left\{\left[\rho_s\frac{\partial\Phi_s}{\partial r}\right]\left(f_\rho\,g\right) - \left[\rho_s\Phi_s\right]\left[\frac{1}{\delta}\frac{d\delta}{dr}\right]\,\left(\eta\,f_\rho\,\frac{dg}{d\eta}\right)\right\}.
\end{aligned} \tag{181}$$

We note that the term in curly brackets on the right-hand-side is exactly equation 141, so we can plug it directly into the Gauss equation for $\partial\Phi/\partial r$ using equation 141. This is our special trick which made the momentum integral derivation possible in the main body of the paper, so here we use it for the transformed similarity equations.

First we divide the entire equation by $\rho_s V_{sr}^2/r$ to obtain:

$$\left[\frac{\partial}{\partial \ln r}\ln\left\{r\rho_s V_{sr}^2\right\}\right]\left(f_\rho\, F_r^2\right) \;-\; \eta\frac{d}{d\eta}\left(f_\rho\, F_r^2\right) \tag{182}$$
$$+\left[\frac{1}{\rho_s V_{sr}^2}\,\frac{\partial}{\partial\phi}\left\{\rho_s\, V_{s\phi}\, V_{sr}\right\}\right]\left(f_\rho\, F_\phi F_r\right)+\left[\frac{V_{sz}}{V_{sr}}\right]\left[\frac{r}{\delta}\right]\;\frac{d}{d\eta}(f_\rho\, F_r\, F_z)$$
$$-\left[\frac{V_{s\phi}^2}{V_{sr}^2}\right]\left(f_\rho\, F_\phi^2\right)$$
$$=-\left[\frac{\Phi_s}{V_{sr}^2}\right]\left\{\left[\frac{\partial\ln\Phi_s}{\partial\ln r}\right](f_\rho g)-\left(\eta\, f_\rho\,\frac{dg}{d\eta}\right)\right\}.$$

Now we need to define the coefficients of our similarity relations which in principle could be galaxy specific; i.e. different for each galaxy depending on its history and initial conditions. Since these conditions are unknown, we denote this possible dependence by *. So we define:

$$\left[\frac{V_{s\phi}^2}{V_{sr}^2}\right] \;=\; A(*), \tag{183}$$
$$\left[\frac{\partial}{\partial\ln r}\ln\left\{r\rho_s V_{sr}^2\right)\right\}\;=\; B(*), \tag{184}$$
$$\left[\frac{1}{\rho_s V_{sr}^2}\,\frac{\partial}{\partial\phi}\left\{\rho_s\, V_{s\phi}\, V_{sr}\right\}\right]\;=\; C(*), \tag{185}$$
$$\left[\frac{V_{sz}}{V_{sr}}\right]\;=\; D(*),\;\left[\frac{d\delta}{dr}\right] \tag{186}$$
$$\left[\frac{\Phi_s}{V_{s\phi}^2}\right]\;=\; E(*). \tag{187}$$

So substituting these into equation 182 yields:

$$\left[\Phi_s\right]\left\{\left[\frac{\partial\ln\Phi_s}{\partial\ln r}\right](f_\rho\, g)-\left(\eta\, f_\rho\,\frac{dg}{d\eta}\right)\right\} \tag{188}$$
$$=\left[V_{sr}^2\right]\left\{B\;\left(f_\rho\, F_r^2\right)\;-\eta\frac{d}{d\eta}\left(f_\rho\, F_r^2\right)\right.$$
$$\left.+C\;\left(f_\rho\, F_\phi F_r\right)+D\,\frac{d}{d\eta}(f_\rho\, F_r\, F_z)-A\;\left(f_\rho\, F_\phi^2\right)\right\}$$
$$=-\left[\frac{V_{s\phi}^2}{A}\right]\left\{B\;\left(f_\rho\, F_r^2\right)\;-\eta\frac{d}{d\eta}\left(f_\rho\, F_r^2\right)\right.$$
$$\left.+C\;\left(f_\rho\, F_\phi F_r\right)+D\,\frac{d}{d\eta}(f_\rho\, F_r\, F_z)-A\;\left(f_\rho\, F_\phi^2\right)\right\}. \tag{189}$$

Now we need to re-write the right-hand-side as $\partial\Phi/\partial r$ using equation 141, then substitute it into Gauss' equation. This will bring the density into the

problem along with the ϕ, η-terms from Gauss's law. Then we will integrate that over η.

Collecting the terms for the Gauss gravitational law yields:

$$\begin{aligned}
&\frac{1}{r}\frac{\partial}{\partial r}\left\{\Phi_s\left[\frac{\partial \ln \Phi_s}{\partial \ln r}\right](g) - \left[\Phi_s \frac{d\ln\delta}{d\ln r}\right]\left(\eta\frac{dg}{d\eta}\right)\right\} \\
&+\left[\frac{1}{r^2}\frac{\partial^2\Phi_s}{\partial\phi^2}\right](g) \;+\; \left[\frac{\Phi_s}{\delta^2}\right](\frac{d^2g}{d\eta^2}) \\
&= 4\pi\, G\, [\rho_s]\,(f_\rho). \qquad (190)
\end{aligned}$$

Substituting from equation 182 leaves:

$$\begin{aligned}
&-\frac{1}{A}\left\{B\,\left(f_\rho\, F_r^2\right) - \eta\frac{d}{d\eta}\left(f_\rho\, F_r^2\right) + C\,\left(f_\rho\, F_\phi F_r\right)\right. \\
&\qquad \left. +D\,\frac{d}{d\eta}(f_\rho\, F_r\, F_z) - A\,\left(f_\rho\, F_\phi^2\right)\right\}\left[\frac{1}{r}\frac{\partial}{\partial r}V_{s\phi}^2\right] \\
&+E\left[\frac{1}{r^2}\frac{\partial^2 V_{s\phi}^2}{\partial\phi^2}\right](g) \;+\; E\left[\frac{V_{s\phi}^2}{\delta^2}\right](\frac{d^2g}{d\eta^2}) \\
&= 4\pi\, G\,[\rho_s](f_\rho). \qquad (191)
\end{aligned}$$

Note that although this equation is by definition independent of r, it is still dependent on η and ϕ. We will eliminate the η-dependence by integrating over η across the galaxy. For the term in curly brackets we define:

$$\begin{aligned}
&Q(A,B,C,D,E) = \qquad (192) \\
&-A\int_{-\infty}^{\infty} d\eta \left\{B\,\left(f_\rho\, F_r^2\right) - \eta\frac{d}{d\eta}\left(f_\rho\, F_r^2\right)\right. \\
&\qquad \left. +C\,\left(f_\rho\, F_\phi F_r\right) + D\,\frac{d}{d\eta}(f_\rho\, F_r\, F_z) - A\,\left(f_\rho\, F_\phi^2\right)\right\}.
\end{aligned}$$

where everything to the right of $d\eta$ is to be integrated over $d\eta$. Clearly Q is just a constant which is specific to each galaxy (since it depends on the profiles of density and velocity which in turn depend on the starred constants). Note that the dominant contribution is probably the last term, the integral over the profile of ρV_ϕ^2. Clearly non-zero values of V_r could change Q significantly. Only by considering actual profiles for f_ρ, F_ϕ, F_r, F_z, can we determine whether the Q increases or decreases if V_r is significant.

Now consider the last term on the left-hand-side of equation 191:

$$\int_{-\infty}^{\infty}\frac{d^2g}{d\eta^2}(\eta)d\eta = \left.\frac{dg}{\partial\eta}\right|_{-\infty}^{\infty}. \qquad (193)$$

If the galaxy is symmetrical in η, this term will vanish identically. If not it may vanish anyway if its r-dependent coefficient vanishes. We will examine that separately below.

Now consider the integral of next to the last term on the left-hand-side of equation 191:

$$E\left[\frac{1}{r^2}\frac{\partial^2 V_{s\phi}^2}{\partial\phi^2}\right]\int_{-\infty}^{\infty} g(\eta)d\eta. \tag{194}$$

Unless the galaxy is anti-symmetrical (which seems unlikely), the integral is not zero. So it is the double partial derivative with respect to ϕ that determines whether this term must be included. We will deal only with azimuthally averaged quantities (since that is most if not all of the data), so we only need consider:

$$\frac{1}{2\pi}\int_0^{2\pi}\left[\frac{\partial^2 V_{s\phi}^2}{\partial\phi^2}\right]d\phi = \frac{1}{2\pi}\left\{\frac{\partial}{\partial\phi}V_{s\phi}^2\Big|_{2\pi} - \frac{\partial}{\partial\phi}V_{s\phi}^2\Big|_0\right\} = 0. \tag{195}$$

So since it is periodic by hypothesis, no matter the Fourier decomposition of V_ϕ, this term vanishes identically in the equation average over ϕ.

So if we average equation 191 over ϕ and integrate it from $-\infty < \eta < \infty$ leaves us with just:

$$\left\{Q\int_{-\infty}^{\infty} f_\phi^2(\eta)d\eta\right\}\left\{\frac{1}{r}\frac{\partial}{\partial r}\left[\delta(r)\,\overline{\overline{V^2}}_{s\phi}(r)\rangle\right]\right\} = 4\pi\,G\left\{\int_{-\infty}^{\infty} d\eta\, f_\rho(\eta)\left[\delta(r)\,\overline{\overline{\rho_s}}(r)\rangle\right]\right\}, \tag{196}$$

where here we use the double overline to denote averaging over ϕ only; i.e.,

$$\overline{\overline{V^2}}_{s\phi} = \left\{\frac{1}{2\pi}\int_0^{2\pi} d\phi\left[V_{s\phi}^2(r,\phi)\right]\right\}, \tag{197}$$

$$\overline{\overline{\rho}}_s(r)\rangle = \left\{\frac{1}{2\pi}\int_0^{2\pi} d\phi\,\rho_s(r,\phi)\right\}. \tag{198}$$

Note that the term in curly brackets on the right-hand-side of equation 196 is exactly the two-dimensional integrated density, $\langle\rho\rangle$, which is cited in most data sets and used in the main body of the paper. Also $\overline{\overline{V^2}}_{s\phi}$ does not in general equal $\overline{\overline{V}}_{s\phi}^2$, but in the absence of evidence to the contrary we shall ignore (for now) the difference. (Note also that there is a slight difference from the main body of the text since there we integrated over z. The difference appears in the δ in front of the integral.) Note that all the terms in Q involving E have fallen out of the equation due to symmetry and averaging over ϕ.

So we are left with:

$$\left\{\frac{1}{r}\frac{\partial}{\partial r}\left[\delta(r)\,\langle V^2{}_{s\phi}(r)\rangle\right]\right\} = 4\pi\,G\,N\,\overline{\rho}(r), \tag{199}$$

where $N(*)$ is defined to be:

$$N(*) = \left\{ Q \int_{-\infty}^{\infty} f_\phi^2(\eta) d\eta \right\}^{-1}, \tag{200}$$

and contains all the profile dependent constants.

We can integrate equation 199 to obtain:

$$\delta(r) \left[\overline{\overline{V^2}}_{s\phi}(r) - \overline{\overline{V^2}}_{s\phi}(r_o) \right] = 4\pi G\, N \int_{r_o}^{r} \langle \rho_s(r') \rangle r' dr'. \tag{201}$$

The $\langle \rho_s(r) \rangle$ is just the azimuthally-averaged density integrated over the layer; i.e., the quantity that is usually measured and reported. Note that there are two contributions to the r-dependence of $\langle \rho \rangle$: the r-variation of the azimuthally-averaged centerline density, $\overline{\rho}_s(r)$; and the spreading of the profile, $\delta(r)$.

We have not yet invoked equation 164, so we define $K(*)$ by:

$$\delta(r) = K(*)\ r. \tag{202}$$

Clearly this gives us the linear relation we obtained for the Milky Way when we plotted the right-hand side of equation 201 divided by $\overline{V^2}_{s\phi}(r)$.

D Interrelation of integral parameters

In fluid mechanics and turbulence integral parameters are quite commonly used. The two most common methods are to define top-hat and/or Gaussian parameters. Both are defined from integrals, but the latter assumes the profile being integrated is a Gaussian. We use both in this paper. This appendix shows how they are related for the cylindrical polar coordinates of interest.

Consider a quantity, say $\rho(r, \phi, z)$ for which we might be only able to access its value integrated over z and averaged over ϕ, say $\langle \rho(r) \rangle$, or only averaged over ϕ, say $\overline{\overline{\rho}}(r, z)$; i.e.,

$$\langle \rho(r) \rangle = \int_{-\infty}^{\infty} dz \left[\frac{1}{2\pi} \int_0^{2\pi} d\phi\, \rho(r, \phi, z) \right] = \int_{-\infty}^{\infty} dz\, \overline{\overline{\rho}}(r, z), \tag{203}$$

where everything to the right of the differentials is to be integrated with respect to that variable. The dimensions of ρ are mass over length-cubed, so the dimensions of $\langle \rho \rangle$ are mass over length-squared. If chose a particular value of $\rho(\cdot)$ as representative, say ρ_{th}, as representative (for example its maximum value), then we can define an integral length scale, say z_t as:

$$z_t(r)\, \rho_{th}(r) = \langle \rho(r) \rangle = \int_{-\infty}^{\infty} dz\, \overline{\overline{\rho}}(r, z). \tag{204}$$

If we know one value somewhere, like $z = 0$, then we can be more precise and choose:

$$\rho_{th}(r) = \overline{\overline{\rho}}(r, 0). \tag{205}$$

This is a particularly useful choice if we actually know the profile peaks at the value, $z = 0$.

Sometimes it is useful to approximate the profile as Gaussian; i.e.,

$$\overline{\overline{\rho}}(z) \approx \overline{\overline{\rho}}(0)\, e^{-z^2/2\sigma_z^2}. \tag{206}$$

Now we can actually find the relation between the top-hat parameter, $z_m(r)$, and the Gaussian standard deviation parameter, say $\sigma_z(r)$ since:

$$z_t(r)\rho_{th}(r) = \int_{-\infty}^{\infty} dz\, \overline{\overline{\rho}}(0) e^{-z^2/2\sigma_z(r)^2} = \overline{\overline{\rho}}(0)\, \sqrt{2\pi}\ \sigma_z(r). \tag{207}$$

The integral is easily evaluated leaving us with:

$$z_t(r) = \sqrt{2\pi}\ \sigma_z(r). \tag{208}$$

We will find this relation particularly useful since the galaxy density profile can be approximated as Gaussian in z (e.g., Figure 14 of [3]). For the velocity profile at this point we can only guess.

References

[1] Abramowitz, M. and Stegun, I. (1964) *Handbook of Mathematical Functions with Formulas, Graphs, and Mathematical Tables*, Dover Books on Mathematics, CUP, Cambridge, UK.

[2] Batchelor, G. K. (1967) 'An Introduction to Fluid Dynamics", CUP.

[3] Bland-Hawthorne, J. and Gerhard, O. (2017) "The Galaxy in Context: Structural, Kinematic and Integrated Properties", arXiv:1602.07702v2 [astro-ph.GA] 5 Jan.2017

[4] Binney, J., & Tremaine, S. 2008, Galactic Dynamics: Second Edition (Princeton University Press)

[5] Castillo, L. and George, W. K. (2001) "Similarity Analysis for Turbulent Boundary Layer with Pressure Gradient: Outer Flow", *AIAA Journal*, 39, 1, doi.org/10.2514/2.1300

[6] Castillo, L. Wang, X. and George, W. K. (2004) "Separation Criterion for Turbulent Boundary Layers Via Similarity Analysis" *J. Fluids Eng.* 126(3): 297-304.

[7] Corbelli, E. (2023) "private communication to WKG"., March 2023.

[8] Corbelli, E., Salucci, P. (2000) "The extended rotation curve and the dark matter halo of M33". *Monthly Notices of the Royal Astronomical Society*. 311 (2): 4414457. arXiv:astro-ph/9909252. doi:10.1046/j.1365-8711.2000.03075.x.

[9] Corbelli, E., Thiker, D., Zibetti, S., Giovanardi, C and Salucci, P. (2014) "Dynamical signature of a ΛCDM-halo and the distributions of baryons in M33., *AA, 572*, A23, doi 10:1051/0004-6361/201424033.

[10] Danaila, L. Voivenel, L. and Varea. E. (2017) "Self-similarity criteria in anisotropic flows with viscosity stratification", *Phys, Fluids*, 29, 2.

[11] Eilers, A-C, Hogg, D.W., Rix, H-W., and Ness, M.K. (2018) "The circular velocity curve of the Milky Way from 5 to 25 kpc", arXiv:1810.09466v2 [astro-ph.GA], 4 Dec. 2018.

[12] Ewing, D., Frohnapfel, B., George, W.K., Pedersen, J.M. and Westerweel, J.(2007) "Two-point similarity the the round-jet," *J. Fluid Mechanics , 577*, 309 - 330 (https://doi.org/10.1017/S0022112006004538).

[13] George, W.K. (1989) "The self-preservation of turbulent flows and its relation to initial conditions and coherent structures" *Advances in turbulence* (George W.K. and Arndt, R E A. eds), Springer (available at wwww.turbulence-online.com)

[14] George, W.K. and L. Castillo (1997) "Zero-pressure gradient turbulent boundary layer", *Appl. Mech. Rev.* Dec 1997, *50*(12): 689-729

[15] George, W.K.(2012) "Asymptotic Effect of Initial and Upstream Conditions on Turbulence" *J. Fluids Eng.134*,6: 061203 (27 pages) (https://doi.org/10.1115/1.4006561)

[16] George, W.K.(1990) "Governing equations, experiments, and the experimentalist" *Elsevier Experimental Thermal and Fluid Science, 3*, 6, 557-566 (https://doi.org/10.1016/0894-1777(90)90071-E)

[17] George, W.K. (2013) "Lectures in Turbulence for the 21st Century", http://www.turbulence-online.com/Publications/Lecture Notes/Turbulence Lille/TB 16January2013.pdf.

[18] George, W. K., Abrahamsson, H. Eriksson, J. Karlsson, R. and Löfdahl, L. and Wosnik, M. "A similarity theory for the turbulent plane wall jet without external stream", *J. Fluid Mech.*, 425 DOI:10.1017/S002211200000224X

[19] Galaxy Book: https://galaxiesbook.org/chapters/II-01.-Flattened-Mass-Distributions.html

[20] George, W.K. and Johansson, T.J. (2022) "An Alternative Cosmological Model for an Expanding Universe" (http://www.turbulence-online.com/Publications/Purdue April 2022 Paper.pdf)

[21] Guelph Physics (https://www.physics.uoguelph.ca/chapter-12-greens-function.)

[22] Hogg, D. W. Eilers, A. C. & Rix, H. W. (2018) "Spectrophotometric parallaxes with linear models: Accurate distances for luminous red-giant stars" ArXiv e-prints, arXiv:1810.09468

[23] Hultmark, M. (2012)"A theory for the streamwise turbulent fluctuations in high Reynolds number pipe flow" *J. of Fluid Mechanics*, 707, 575 - 584, DOI: 10.1017/jfm.2012.307

[24] Ivanov, G. R. and Kunchev, P. Z. (1985) "On the spiral structure of M33 ", *Astrophys. Space Sci.*, 116, 341-348. (https://doi.org/10.1007/BF00653788)

[25] Misiriotis, A. , Kilouris, E. M. Papamastorakis, J. Bourmis, P. and Goudis, C. D. (2006) "The distribution of the ISM in the Milky Way", *A &A* 459, 113–123 DOI: 10.1051/0004-6361:20054618

[26] Jeans, J. H. (1915), *MNRAS*, 76, 70

[27] Johansson, P. B. V., George, W.K. and Gorlay, M. 2003 "Equilibrium similarity, effects of initial conditions and local Reynolds number on the axisymmetric wake", *Physics of Fluids 15*, 603–617 (https://doi.org/10.1063/1.1536976)

[28] Lighthill "Generalized Functions"

[29] Lumley, J. L. (1970)"Stochastic Tools in Turbulence, Academic Press.

[30] López Fune, E., Salucci, P. and Corbelli, E. (2017) "Radial dependence of the dark matter distribution in M33", *Roy. Astron. Soc. MNRAS 468*, 147-153 .

[31] McGaugh, S., Lelli, R., and Schombert, J. M. (2016) "Radial Acceleration in Rotational Supported Galaxies", *PRL 117*, 201101.

[32] Moser, R. D. Rogers, M. M. and Ewing, D. W. (1998) "Self-similarity of time-evolving plane wake", *J. Fluid Mechanics* 367, 255-289.

[33] Oort, J.H. (1922) "Some Peculiarities in the Motion of Stars of High Velocity,' *Bull. Astron. Inst. Neth. 1*, 133–37 .

[34] Rogers, M. (2002) "The evolution of strained turbulent plane wakes", *J. Fluid Mechanics", 463*, 53-120.

[35] Rubin, V. and Ford, W.K. (1970) "Rotation of the Andromeda Nebula from a Spectroscopic Survey of Emission Regions", *Astrophysical Journal 159: 379.*

[36] Shiri, A., George, W.K. and Naughton, J. W. (2008) "Experimental Study of the Far Field of Incompressible Swirling Jets", *AIAA, 46*, 8, 2002-2009.

[37] Fitzpatrick, R. 2023 "Poisson's Equation in Cylindrical Coordinates", *Lecture Notes in Electricity and Magnetism.* https://farside.ph.utexas.edu/teaching/jk1/Electromagnetism/node37.html)

[38] Watson, G. N. (1922) *A Treatise on the Theory of Bessel Functions*, CUP, Cambridge, UK.

[39] NASA/JPL-Caltech/R. Hurt (2011), "Artist conception of the Milky Way", *Wiki*, (https://commons.wikimedia.org/wiki/)

[40] "Galaxy rotation curve" Wikipedia, (https://en.m.wikipedia.org)

[41] (https://en.wikipedia.org/wiki/Root system/media/File:Root system A1xA1.svg)

[42] Wiki Bessel

[43] Wosnik, M. Castillo, L. and George, W. K. (2000) "A theory for turbulent pipe and channel flows" *J. Fluid Mech.*, 421, 115–145.

[44] Wosnik M. and Dufresne N. (2013) "Experimental investigation and similarity solution for the axisymmetric turbulent wake with rotation", *Proceedings of ASME Fluids Engineering Division Summer Meeting 2013*, Paper FED2013-16565, July 7-13, 2013, Incline Village, NV. https://doi.org/10.1115/FEDSM2013-16565

[45] Zwicky, F. (1933), "Die Rotverschiebung von extragalaktischen Nebeln" [The red shift of extragalactic neubulae], *Helvetica Physica Acta (in German), 6*: 110–127

Figures

Figure 1: Galaxy M33 showing the visible matter, the measured azimuthal velocities and the theoretical calculation using the Gauss-Newton equations. The difference between 'expected' and observations is usually attributed to dark matter' (Data from [8], Figure from [40].)

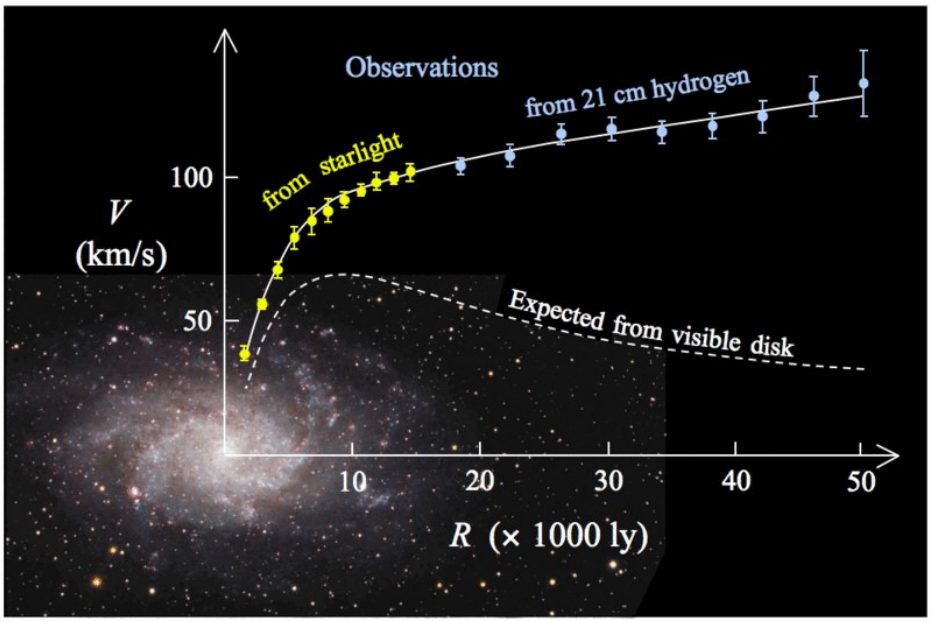

Figure 2: Three galaxies from McGaugh et al. [31]. Their caption is below the figure. The black symbols the measured azimuthal velocities, and the solid lines are the velocities calculated from the observed mass and the Gauss-Newton equations. The difference is presumed to be due to either 'Dark Matter' or the need for alternative gravity.

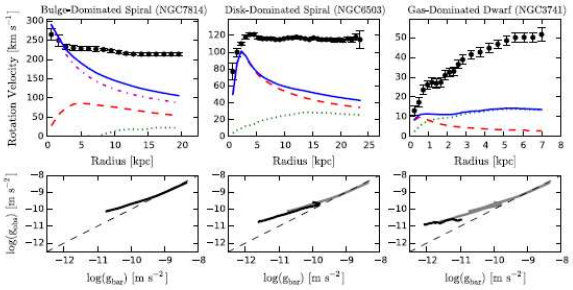

FIG. 2. Examples of mass models and rotation curves for individual galaxies. The points with error bars in the upper panels are the observed rotation curves $V(R)$. The errors represent both random errors and systematic uncertainty in the circular velocity due to asymmetry in the velocity field. In all galaxies, the data exceed the lines $v_{\rm bar} = \sqrt{R g_{\rm bar}}$ representing the baryonic mass models [Eq. (3)], indicating the need for dark matter. Each baryonic component is represented: dotted lines for the gas, dashed lines for the stellar disk, and dash-dotted lines for the bulge, when present. The sum of these components is the baryonic mass model (solid line). The lower panels illustrate the run of $g_{\rm bar}$ and $g_{\rm obs}$ for each galaxy, with the dashed line being the line of unity. Note that higher accelerations occur at smaller radii. From left to right each line is replotted in gray to illustrate how progressively fainter galaxies probe progressively lower regimes of acceleration.

Figure 3: Data for Milky Way from Eilers et al.[11] for V_ϕ, V_r and the circular velocity calculated from Jeans equation along with various solutions to their versions of the galactic equations. Their caption is below figure. The large error bars are typical for astronomical data.

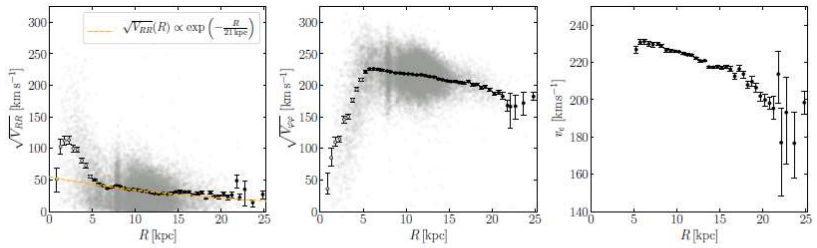

Figure 1. Radial profiles of the components of the velocity tensor $\sqrt{V_{RR}}$ (left panel), $\sqrt{V_{\varphi\varphi}}$ (middle panel), and the circular velocity v_c (right panel). The small grey dots show individual stars, whereas the black data points show the ensemble averaged values with uncertainties determined via bootstrapping with 100 samples. We exclude all stars within a distance of $R < 5$ kpc from the Galactic center (open data points) from our analysis due to the presence of the Galactic bar.

Figure 4: Data for circular velocity for Milky Way from Eilers et al.[11] along with various solutions to Jeans equation. Their caption is below the figure. Note that none of the computations come close to the measurements without including dark matter. The large error bars are typical for astronomical data and computations.

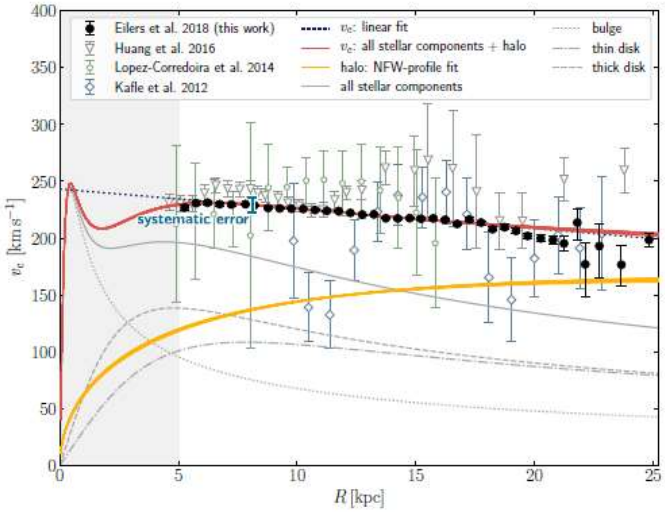

Figure 3. The new measurements of the circular velocity curve of the Milky Way are shown as the black data points. The errorbars are estimated via bootstrapping and do not include any systematic uncertainties. We note the systematic error at the location of the Sun, which influences our results at the $\lesssim 3\%$ level (see § 5.2). The blue dotted curve shows a linear fit to our data (Eqn. 7), whereas the red curves show 100 random draws from the posterior distribution of the fit parameters to the circular velocity modeled as a sum of stellar components, i.e. bulge, thin and thick disk (grey curves), and a dark matter halo estimated by an NFW-profile (yellow curves, also showing 100 random draws from the posterior). The measurements of various other studies of the circular velocity are shown as colored data points. The light grey shaded region marks the region, where dynamics are strongly influenced by the Milky Way's bar.

Figure 5: Figure showing the streamlines computed from the velocities of Eilers et al. [12] (reproduced as Figure 3 here) and super-imposed on the Milky Way image of [39].

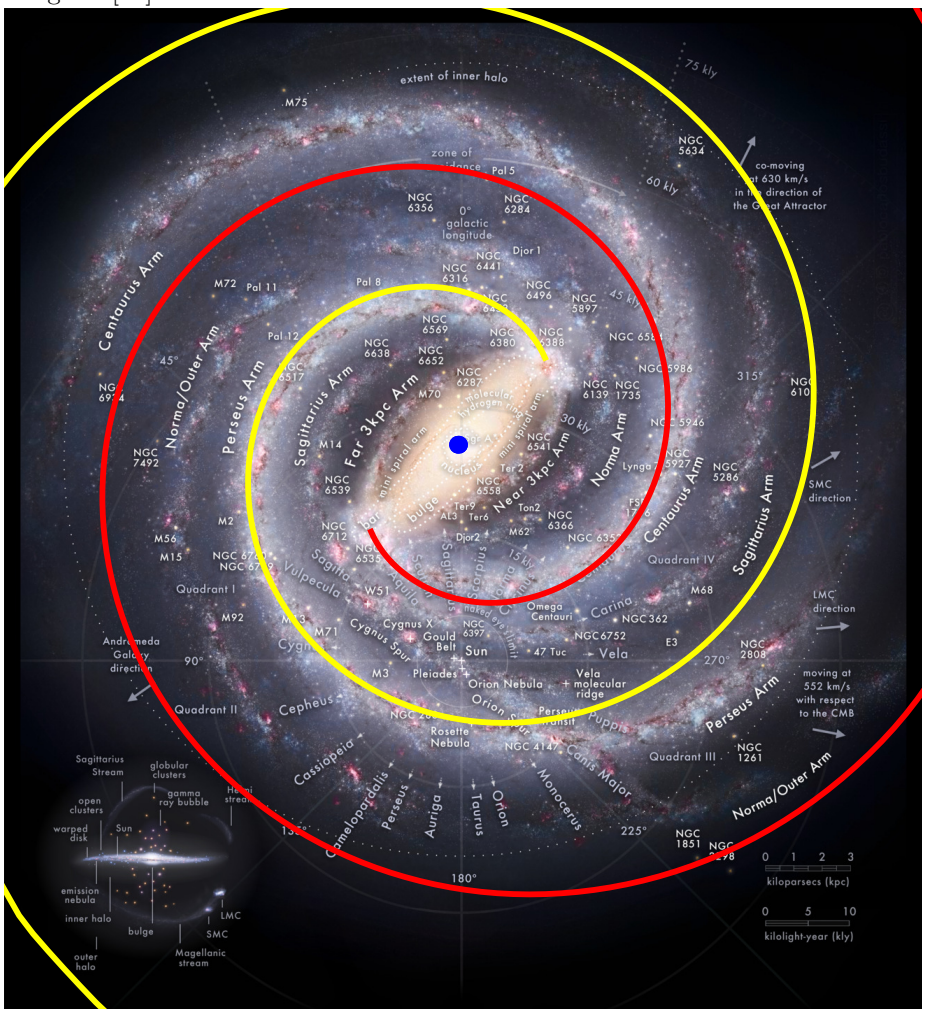

Figure 6: Figure showing the velocity streamlines using data from Figure 2 of Eilers et al. [11] (reproduced here as Figure 3) along with spiral produced using constant values of the velocity ratio, $V_\phi/V_r = 6.5$. The latter is a true log spiral, $\phi_s(r) - \phi_s(0) = 6.5\, ln\, r/r_o$. Note that this plot does not include the core region of the previous plot since these data go out to much larger radius ($r = 25$ kpc).

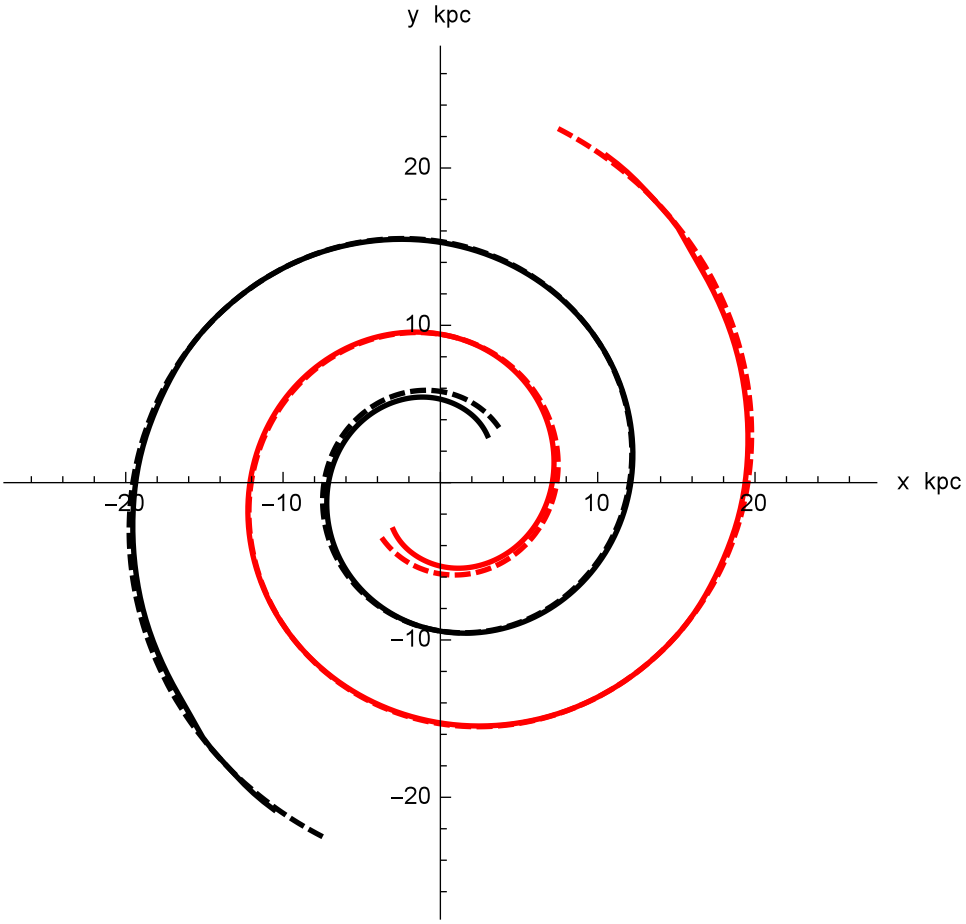

Figure 7: Plot of V_ϕ/V_r versus r for data of [11] showing that it appears to be asymptotically constant at $V_\phi/V_r \approx 6.5$.

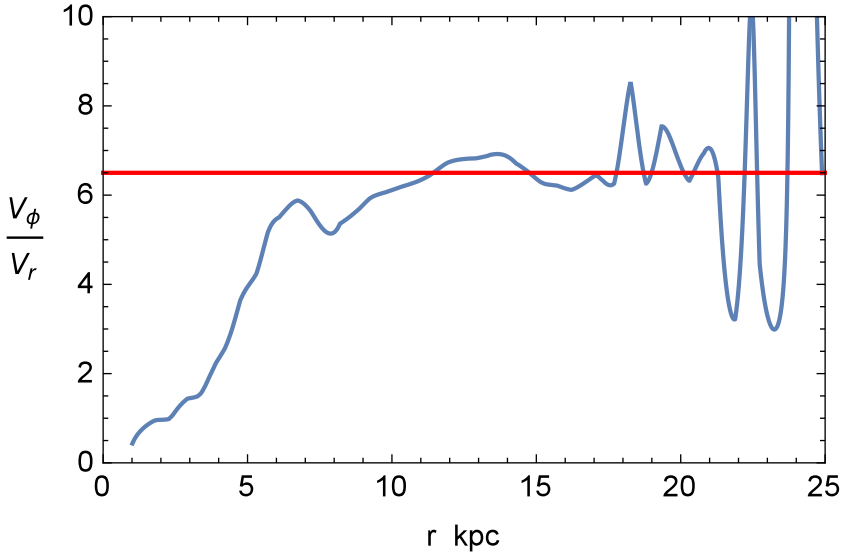

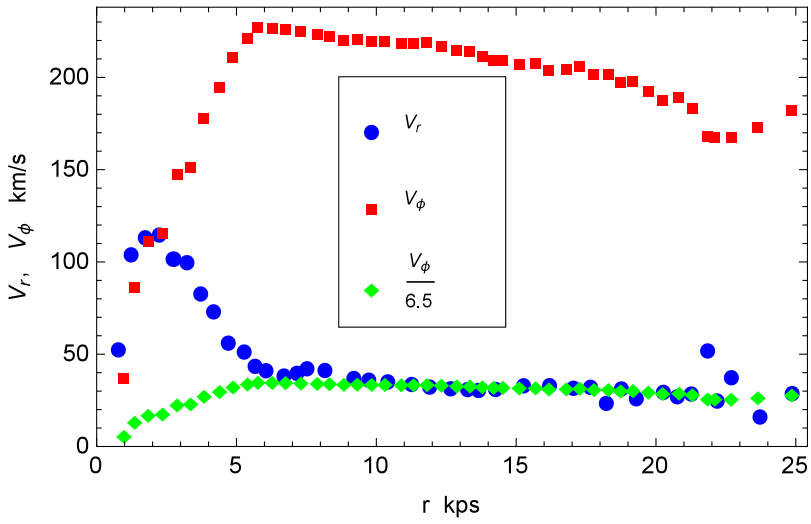

Figure 8: Profiles of $V_\phi(r)$ and $V_r(r)$ (same as in Figure 2) but also plotting $V_\phi(r)/6.5$ on top of $V_r(r)$. This is not a fit to V_r, but a prediction of the similarity theory which does not seem to have been previously noticed.

Figure 9: Plots showing how the running mass, $M_g(r)$, for M33 computed form the measured $\langle \rho_{stars} \rangle$ and $\langle \rho_{gas} \rangle$ increases with radius, r. Data of Corbelli et al. [9].

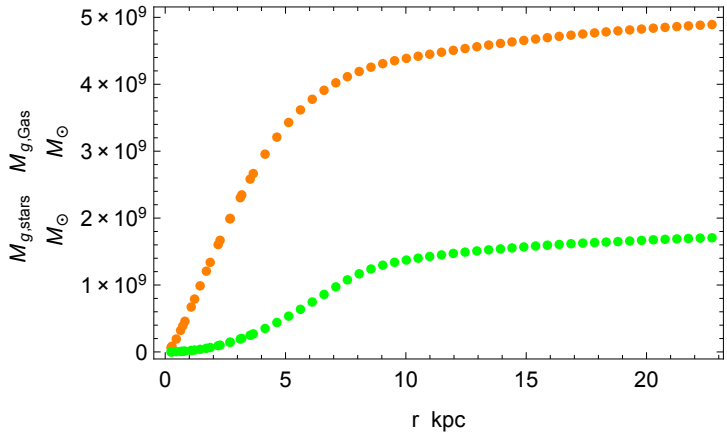

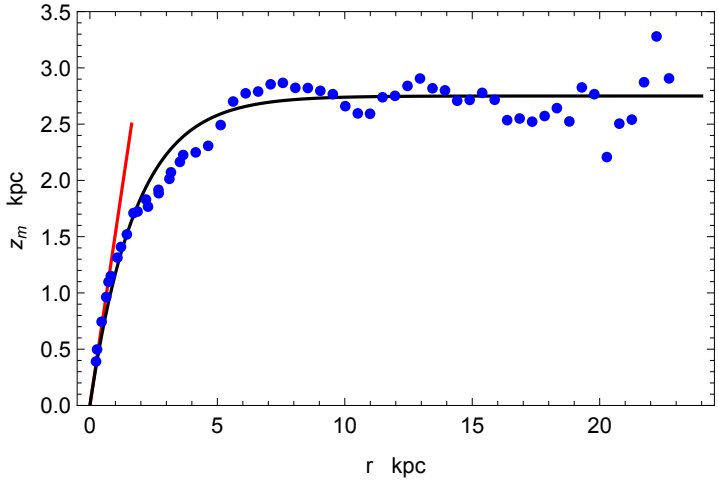

Figure 10: The momentum thickness, z_m, for M33 computed using V_ϕ data and the star density data, $\langle \rho_{stars} \rangle$, of Corbelli et al. [9] in equation 34. The data have been computed using the measured V_ϕ and M_g shown in Figure 9 and computed from the measured $\langle \rho \rangle_{stars}$ only. The straight (red) line indicates the low r similarity regime for which $z_m \propto r$; the other similarity regime corresponds to z_m asymptotically constant. The solid black line is an interpolation consistent with both fits, $z_m = 2.75(1 - exp(-r/1.8))$.

Figure 11: Figure showing how the V_ϕ data for $M33$ of Corbelli et al. [9] can be reconstructed from equation 34 using a constant $z_m = 2.75$ (dashed red line) and also using the composite fit $z_m = 2.75(1 - exp(-r/1.8))$ (solid blue line) shown in Figure 10.

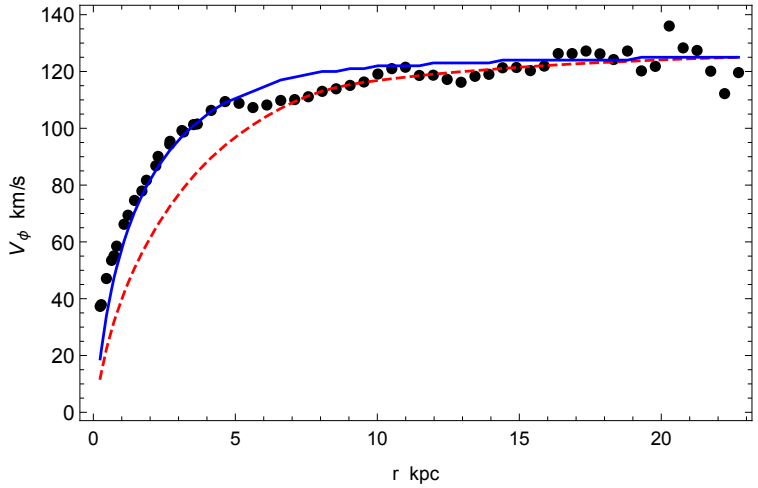

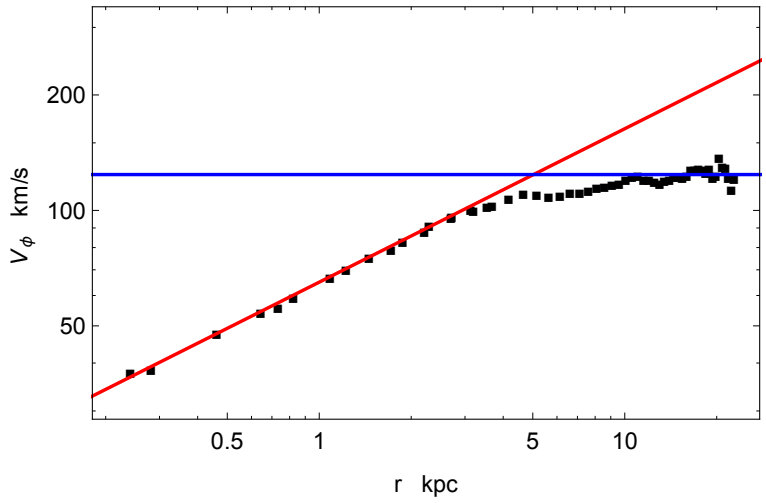

Figure 12: Log log plot of the V_ϕ data for M33 of Corbelli et al. [9] showing two regions: a $r^{0.4}$ for low values of r, and a constant asymptote for high r values.

Figure 13: Plot showing the ratio of $\langle \rho_{stars} \rangle$ to $\langle \rho_{gas} \rangle$ versus radius for M33 using data of Corbelli et al. [9]

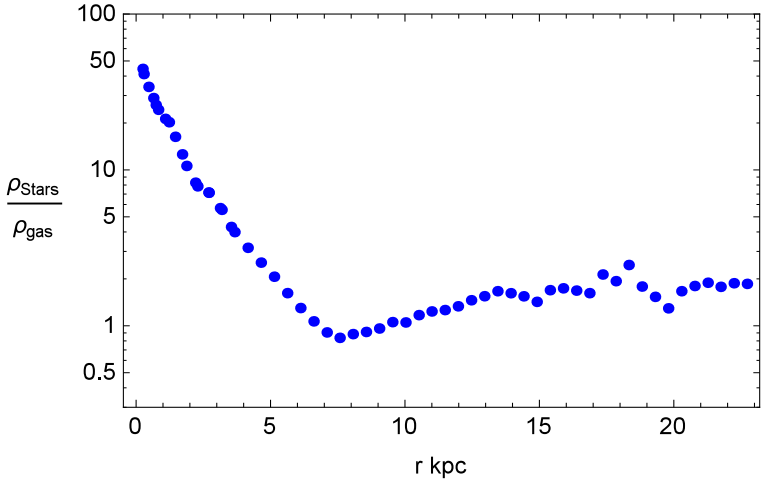

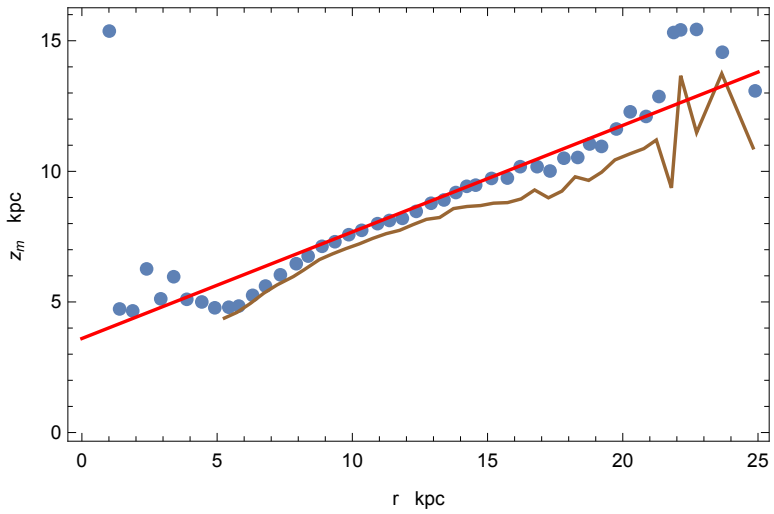

Figure 14: Figure showing the momentum thickness, z_m, for the Milky Way computed using the data of Eilers et al. [11] in equation 34. The solid (blue) disks are computed using V_ϕ only. The jagged line shows z_m computed using V_c, the 'circular velocity' of [11]. The red line is a linear fit: $z_m = 3.6 + 0.4\,r$.

Figure 15: Figure for Milky Way showing the measured velocity of Eilers et al. [11] for V_ϕ along with the the velocity back-calculated using the same mass distribution and the linear fit to z_m.

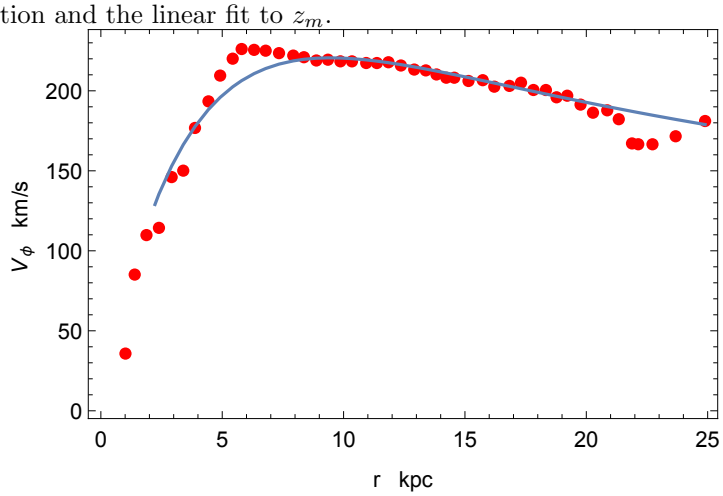

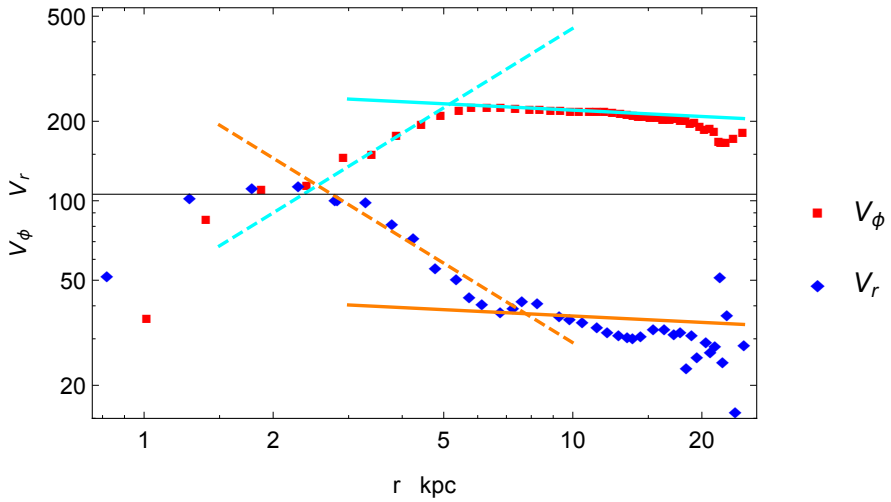

Figure 16: Figure showing log-log plots of V_ϕ and V_r for the Milky Way along with lines identifying possible power law regions. The dashed lines correspond to slopes of +1 and -1. The solid lines have slope 0.08.

Figure 17: Figure showing linear-linear plots of V_ϕ and V_r for the Milky Way along with lines identifying high r similarity region in both. The green line is the power law of the preceding figure. Also shown are linear fits to V_ϕ (blue) and V_r (orange) for $r > 5$.

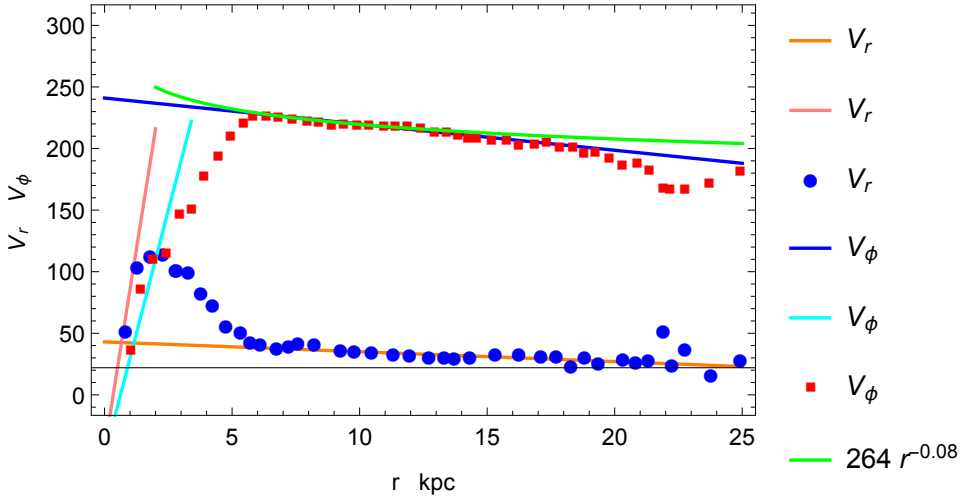

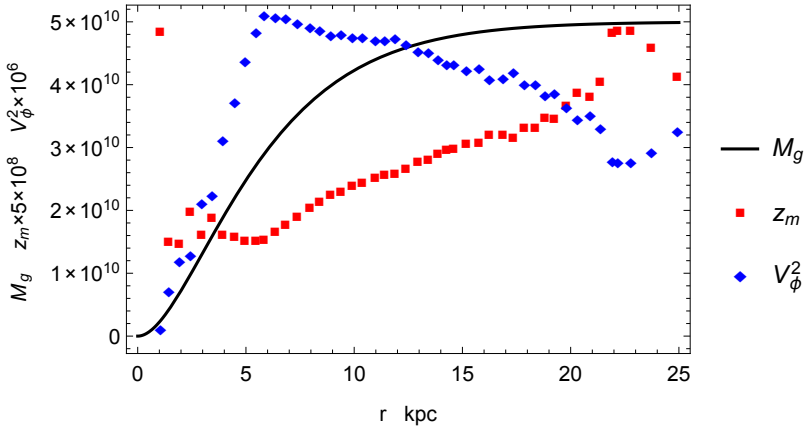

Figure 18: Plot showing how mass distribution (black line) in Milky Way corresponds to similarity region in V_ϕ (blue diamonds) and z_m (red squares).